J. Fluid Mech. (1993), *vol.* 251, *pp.* 109–148

Turbulent shear flow over slowly moving waves

By S. E. BELCHER AND J. C. R. HUNT

Department of Applied Mathematics and Theoretical Physics, University of Cambridge, Silver Street, Cambridge, CB3 9EW, UK

(Received 7 December 1991 and in revised form 1 December 1992)

We investigate the changes to a fully developed turbulent boundary layer caused by the presence of a two-dimensional moving wave of wavelength $L = 2\pi/k$ and amplitude a. Attention is focused on small slopes, ak, and small wave speeds, c, so that the linear perturbations are calculated as asymptotic sequences in the limit $(u_* + c)/U_B(L) \to 0$ (u_* is the unperturbed friction velocity and $U_B(L)$ is the approach-flow mean velocity at height L). The perturbations can then be described by an extension of the four-layer asymptotic structure developed by Hunt, Leibovich & Richards (1988) to calculate the changes to a boundary layer passing over a low hill.

When $(u_* + c)/U_B(L)$ is small, the matched height, z_m (the height where U_B equals c), lies within an inner surface layer, where the perturbation Reynolds shear stress varies only slowly. Solutions across the matched height are then constructed by considering an equation for the shear stress. The importance of the shear-stress perturbation at the matched height implies that the inviscid theory of Miles (1957) is inappropriate in this parameter range. The perturbations above the inner surface layer are not directly influenced by the matched height and the region of reversed flow below z_m: they are similar to the perturbations due to a static undulation, but the 'effective roughness length' that determines the shape of the unperturbed velocity profile is modified to $z_m = z_0 \exp(\kappa c/u_*)$.

The solutions for the perturbations to the boundary layer are used to calculate the growth rate of waves, which is determined at leading order by the asymmetric pressure perturbation induced by the thickening of the perturbed boundary layer on the leeside of the wave crest. At first order in $(u_* + c)/U_B(L)$, however, there are three new effects which, numerically, contribute significantly to the growth rate, namely: the asymmetries in both the normal and shear Reynolds stresses associated with the leeside thickening of the boundary layer, and asymmetric perturbations induced by the varying surface velocity associated with the fluid motion in the wave; further asymmetries induced by the variation in the surface roughness along the wave may also be important.

1. Introduction

We investigate how a deep turbulent boundary layer changes as it passes over a fluid of much greater density when the interface is distorted by a two-dimensional moving wave. Such flows commonly occur both naturally and in engineering. The application of particular interest here is to the wind blowing over the sea, which causes surface waves to be amplified.

In the past 35 years there have been many studies of this problem, often focusing on quantifying the consequential growth rate of the waves. The previous theoretical studies (which include Jeffreys 1925; Miles 1957; Phillips 1957; Townsend 1972, 1980; Jacobs 1987; van Duin & Janssen 1992) have attributed the growth rate to different,

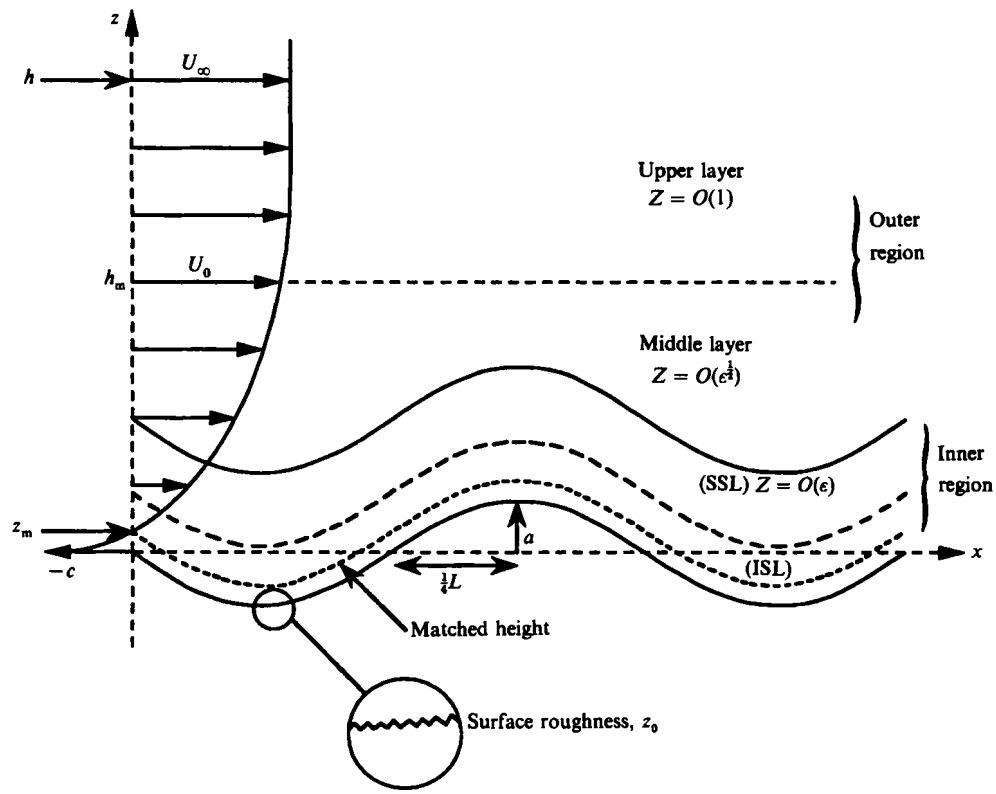

FIGURE 1. Flow geometry and asymptotic structure.

single mechanisms. To date, however, there is no general theory to explain and determine the relative importance of the different processes that control the growth rate over the whole significant ranges of wind and interface wave speeds.

Our approach, which follows most of the previous studies, is to prescribe the interface shape and flow in the water (discussed in §2.1) and then calculate the linear changes to the air flow. As described in §2.2, in the frame of reference that moves with phase speed, c, of the wave crests, the interface shape changes only slowly. For a linear analysis of small changes to the flow, it is shown in §2.3 that the air-flow perturbations can be decoupled into the two independent problems of determining the perturbations caused by the undulating interface shape and the perturbations induced by the variations along the wave of the surface velocity and roughness.

For slowly moving waves, such that $\epsilon = (u_* + c)/U_0 \ll 1$ (where u_* is the unperturbed friction velocity and U_0 is a scale for the unperturbed velocity), both perturbation problems are, as described in §3, analysed using a modified version of the asymptotic theory developed by Hunt, Leibovich & Richards (1988, hereafter referred to as HLR) to describe the changes to a turbulent boundary layer passing over a low hill. Their method derives from the theory of laminar flow over humps (Smith *et al.* 1981) and Townsend's (1965) theory of perturbed turbulent boundary layers. The similarities and differences between the perturbations induced by a moving wave and a fixed hill are discussed in §4.

If k is the wavenumber of the dominant wave, the limit of $\epsilon \to 0$ is equivalent to $kz_0 \to \infty$ with $c/u_* = O(1)$ (see §3.4), which are the same conditions assumed in the asymptotic analyses of van Duin & Janssen (1992) and Jacobs (1987). Although the

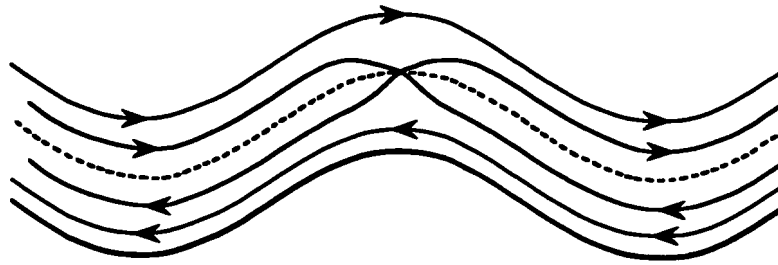

FIGURE 2. Miles' (or critical layer) mechanism of wave growth. A kinematic consequence of the varying pressure perturbation is that, near the matched height, there is a region of recirculating flow, for which Kelvin coined the term 'cat's eyes'.

present analysis has elements in common with these latter studies, it differs in significant ways and our expression for the growth rate has a different magnitude. We have used the analogy with the flow over low hills to understand some aspects of wind waves. The analogy is particularly useful in modelling the changes to the Reynolds stresses, which are well understood in the flow over hills (Sykes 1980; Zeman & Jenssen 1987; Belcher, Newley & Hunt 1993, hereafter referred to as BNH). In particular, BNH have shown that, within the HLR framework, the mixing -length model is appropriate provided it is truncated in the outer region (see §3.1). BNH use this truncated mixing-length model to calculate an analytic formula for the drag on the surface (an integrated effect of the hill), which is in good agreement with results computed using a second-order closure model for the turbulent stresses and with laboratory experiments.

We use the truncated mixing-length model in this study and, in §5, develop an analytical expression for the leading-order energy flux to the wave motions and thence the growth rate of the wave. The magnitudes of the next-order contributions to the energy flux from the various mechanisms are estimated using the results of the analytic model in §7. Since the energy flux is an integrated effect of the wave, we expect that the results will be in good agreement with measurements.

1.1. *Classification of the wave growth mechanisms*

Various mechanisms have been suggested to explain the energy flux from the wind to the waves and hence the amplitude growth rate (refer to figures 1 and 2–8). We focus on the mechanisms that lead to an exponential growth of the waves and propose that these mechanisms be classified as follows.

The perturbations induced by the presence of the undulating wave surface lead to:

M. The Miles (or critical layer) mechanism (figure 2)

Miles (1957) analysed a quasi-inviscid version of the problem: in this model, the role of the Reynolds stresses is confined to the determination of the unperturbed mean velocity profile. For air flowing cocurrently with the waves, there is a height, the critical height, where the unperturbed wind speed equals the wave phase speed. (In the present study, where the effects of the turbulent stresses on the mean motion are considered, following Phillips 1977 we use the term 'matched height'). The upward motion of the air flow over the wave induces a sinusoidal pressure variation which leads to a vortex sheet of periodically varying strength forming at the critical height. Then the 'vortex force' (Lighthill 1962) on the wave leads to a transfer of energy from the wind to the waves. Note that according to this mechanism, the amplitude grows only if the wave is moving, i.e. for a fixed undulation (where the critical layer is at the wave surface) there is no asymmetric pressure and hence no wave growth.

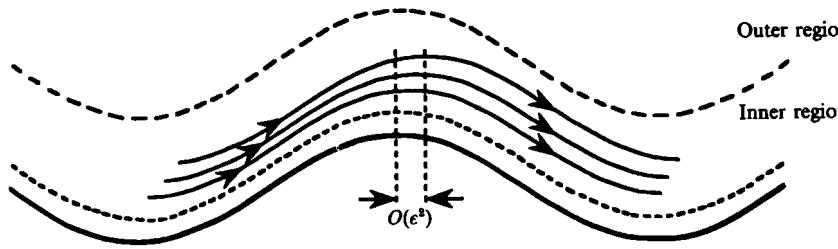

FIGURE 3. Non-separated sheltering growth mechanism. The perturbed boundary layer thickens on the leeside of the crest due to the action of the shear stress in the inner region, thereby leading to a pressure asymmetry in the outer region. (Streamlines above the matched height only are shown.)

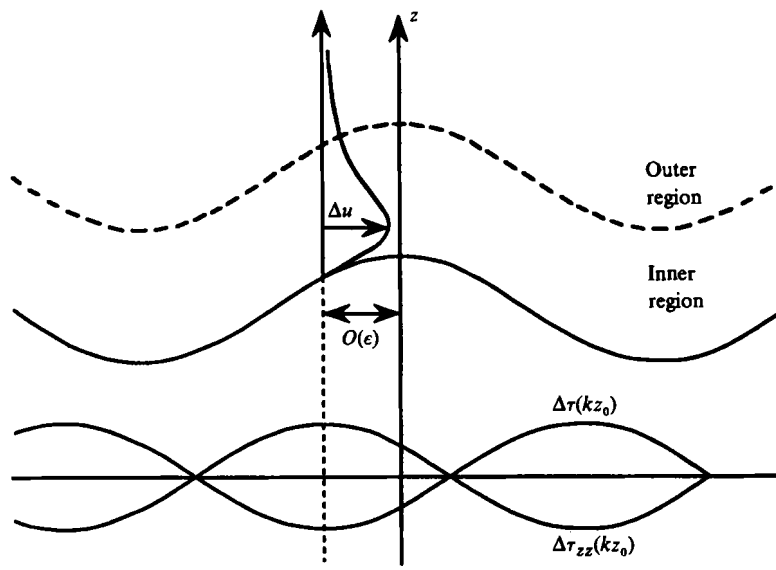

FIGURE 4. Inner-region Reynolds-stress effects on wave growth. Towards the surface the turbulence tends to a local equilibrium structure, so that the Reynolds-stress perturbations are determined by the local velocity gradient. The asymmetry in the inner region leads to perturbations to the Reynolds stresses that are out of phase and hence the Reynolds normal stresses are out of phase at the surface. This also contributes to the energy flux to the wave motion.

NSS. Non-separated sheltering (figure 3)

The action of the Reynolds stresses close to the surface, in the inner region, cause a thickening of the boundary layer on the leeside of wave and thence to mean flow separation when the slope is large enough. The thickness of the inner region is therefore asymmetric and so the, largely inviscid, outer region flow is asymmetrically displaced about the wave, leading to an out-of-phase component to the pressure perturbation. This mechanism is related to Jeffreys' (1925) sheltering hypothesis, which was developed for separated flows over moving waves of large slope to account for their growth.

IRS. Inner-region Reynolds stress effects (figure 4)

Within the inner region, as the surface is approached, the turbulence tends to a local equilibrium so that it adjusts to the local velocity gradient. The asymmetry of the mean flow, and hence the mean flow gradients, in the perturbed boundary layer therefore

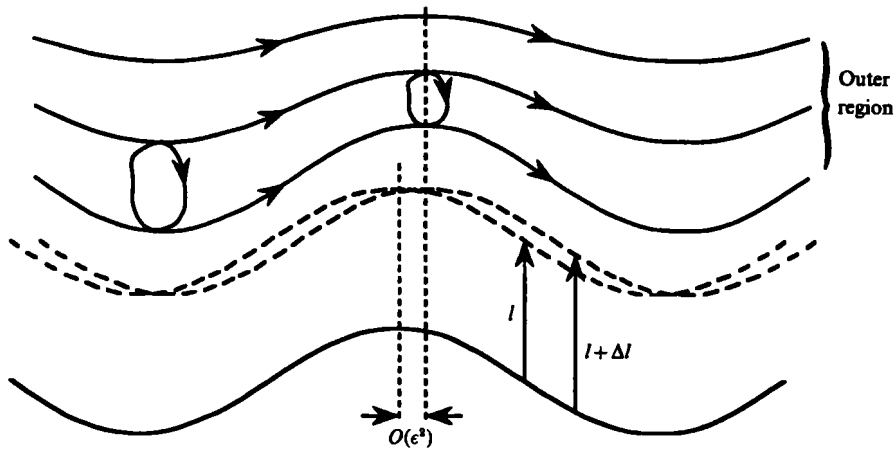

FIGURE 5. Outer-region Reynolds-stress effects on wave growth. The 'non-separated sheltering' in the inner region leads to a change, Δl, in the displacement of the largely inviscid outer-region flow. Consequently, the (rapid) distortion of the Reynolds stresses in the outer region is displaced downwind of the crest, thereby contributing to the energy flux.

lead to asymmetrical perturbations in both the normal and shear Reynolds stresses. These asymmetrical perturbations to the Reynolds stresses at the surface also lead to an amplification of the wave (Townsend 1972, 1980). Stewart (1967) and Longuet-Higgins (1969) have discussed this mechanism for the transfer of energy into the wave motion, but they did not study the effect as part of a systematic analysis.

ORS. Outer-region Reynolds stress effects (figure 5)

The larger eddies in the outer region are bigger than those at lower levels (because of the blocking effect of the surface) and therefore have a longer timescale. Consequently, the distortion to the eddies in this region is determined by the history of the strain by the mean flow, so may be calculated using rapid-distortion theory. Furthermore, the flow in the outer region is displaced slightly downwind of the wave crest by the non-separated sheltering, so that the distortion of the turbulence in the outer region is slightly out of phase with the wave surface. This leads to surface pressure and Reynolds stress perturbations that further induce a growth of the wave. This mechanism was first suggested by the work of Sykes (1980), in a related study of the drag force on a static undulation. The main effect of the curvature of the mean streamlines on the turbulence is also through the rapid-distortion mechanism (Zeman & Jenssen 1987; Belcher 1990), so that this contributes to the wave growth at the same order as the other outer-region Reynolds stress effects.

FAD. Effects of finite-amplitude distortion (figure 6)

At higher values of the wave slope, ak, it may also be significant to consider the asymmetry in the Reynolds stresses produced by a finite-amplitude distortion to the flow. There is a nonlinear drift, of $O((ak)^2)$, of fluid elements and hence the rapid distortion of the turbulence in the outer region is out of phase with the surface (Hunt 1973; Townsend 1980).

The wind over the wave is also affected by the variations in the properties of the water surface and these changes also contribute to the wave growth:

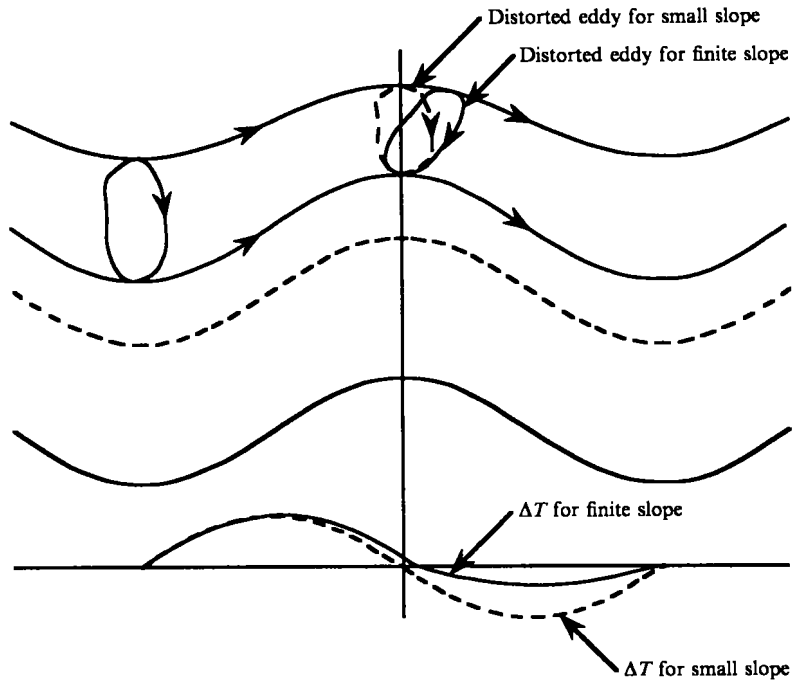

FIGURE 6. Finite-amplitude-distortion effects on wave growth. For larger slopes the distortion (and travel time or drift, ΔT) of the eddies is different along adjacent streamlines and so the distortion is not exactly in phase with the mean streamlines.

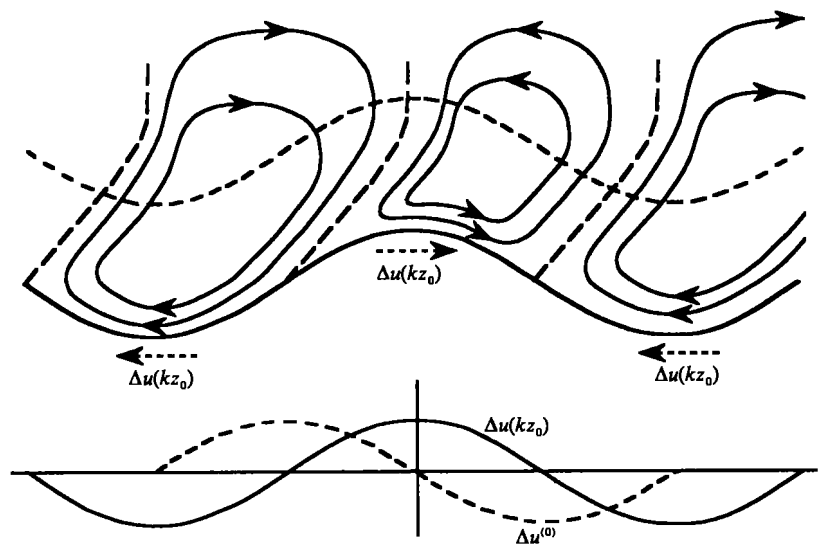

FIGURE 7. Orbital velocity effects on wave growth. The motion of the water at the wave surface generates further perturbations to the air flow. The streamlines of the perturbed flow are sketched. These motions lead to an asymmetric surface-pressure perturbation.

S1. Orbital velocity effects (figure 7)

The motion of the water leads to a varying velocity at the surface of the wave which generates perturbations in the boundary layer above. These perturbations also have asymmetric parts which contribute to the energy flux to the wave motion and thence to a growth of the wave.

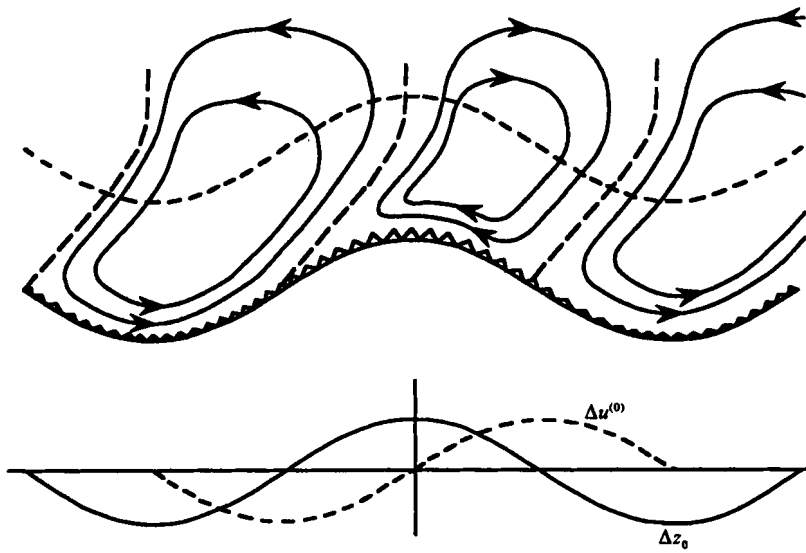

FIGURE 8. Variable-roughness-length effects on wave growth. The perturbations to the air flow caused by the undulating wave shape lead to a varying shear stress along the surface of the wave surface, and thence to a variation in the surface roughness. This leads to further perturbations to the air flow, whose streamlines are sketched, and a further contribution to the asymmetric surface pressure perturbation.

S2. Variable roughness effects (figure 8)

The change of wind speed over the wave induces a variation in the shear stress, τ^*, along the surface and therefore a growth along the wave of small ripples. It is assumed that the wavelength, L, of the dominant wave is much greater than the wavelength of the ripples, λ, which is of order $(\tau^*/\rho_a g)$, so that $\lambda \ll L$. The effect of these ripples on the air flow is equivalent to a variation along the wave in the roughness length, $z_0 \sim \lambda \sim \tau^*/\rho_a g$, which varies because τ^* varies. The variation of z_0 induces further perturbations to the flow which also affect the growth of the wave. A non-uniform roughness length was first included in the numerical calculation of Gent & Taylor (1976).

2. The physical model

The flow domain is composed of two fluids: in $z < 0$ is a fluid (e.g. water) of density ρ_w, which is thought of initially as being at rest; and the region $z > 0$ contains a fluid (e.g. air) of much lower density, ρ_a, which flows as a fully developed turbulent boundary layer in the positive x-direction. We investigate how the boundary layer changes when the interface between the fluids is disturbed by a two-dimensional travelling wave of amplitude a and characteristic wavenumber k. Physically, this models a snapshot of the development of a wave that is in active growth. Alternatively, it may be thought of as modelling the experiments on wind-ruffled mechanically generated waves (e.g. Hsu, Hsu & Street 1981).

2.1. *Flow in the water and interface conditions*

In the present study, the primary aim is to calculate the linear perturbations to the air flow caused by the interface wave. To specify this problem completely, the motion in the water is prescribed to provide boundary conditions on the wind velocity at the wave surface.

To analyse the air flow over a general wave train requires a decomposition into basic wave elements. The wave train is composed of wave packets that, in the absence of the wind, have fixed shape (at least on timescales much larger than the wave period), e.g. the Stokes wave form (see e.g. Kinsman 1984). Each of these wave packets is then analysed separately: the linear solution that we calculate for air flow over one wave packet may be superposed to obtain the solution over a general wave train. For a particular wave packet, the analysis is performed in a frame of reference that moves at the phase speed, c, of the wave packet. The shape of the wave packet is then steady (subject to the constraints mentioned above). Since only the linear perturbations to the air flow are calculated, it is sufficient to analyse the flow over a single Fourier mode. So, without loss of generality, the surface is described by

$$\eta = a\mathrm{e}^{\mathrm{i}kx}; \tag{2.1}$$

it is understood that the real part only is considered. The flow over the complete wave packet is obtained by Fourier superposition. In the particular case of a Stokes wave, the higher harmonics are of $O((ak)^2)$. Our analysis of the linear perturbations to the air neglects terms in the governing equations that are of $O((ak)^2)$, so that, although the air-flow perturbations induced by the higher harmonics of a Stokes-wave shape can be calculated within the present framework, for consistency, the dominant Fourier component only is considered.

In the frame that moves with the crest of the wave packet, the interface shape is, by construction, steady in the absence of the wind. Hence the interface is a streamline. The kinematic boundary condition at the surface is $w^* = -c\,\partial\eta/\partial x$ so that the velocity at the surface, (u^*, w^*), is given by

$$u^* = -c + \bar{u}^*\mathrm{e}^{\mathrm{i}kx}, \quad w^* = -akc\mathrm{i}\,\mathrm{e}^{\mathrm{i}kx} \quad \text{at} \quad z = \eta, \tag{2.2}$$

where $\bar{u}^*$ is a real amplitude. (Superscript * denotes a dimensional velocity.)

In the present study, when a specific form of the motion in the water is required, we suppose, for simplicity, that the motion in the water is given by linear, irrotational, gravity wave theory for small perturbations to deep water with a free surface boundary condition (see e.g. Lighthill 1978, p. 204). Then, moving with the wave crests, the surface boundary condition on the horizontal air speed gives

$$\bar{u}^* = akc. \tag{2.3}$$

Furthermore, the phase speed of the wave is related to k by

$$c = (g/k)^{\frac{1}{2}}. \tag{2.4}$$

As with the wave shape, the $O((ak)^2)$ corrections to (2.2), (2.3) and (2.4) for a Stokes wave can be included without difficulty, but to be consistent with the linearized calculation of the air flow they are not considered here.

For the present purposes of studying the generation of waves by wind, this model of the general wave train as a superposition of freely travelling linear waves is supported by the laboratory measurements of Ramamonjiarisoa (1974, and discussed by Phillips 1977), who measured the phase speeds of the various spectral components of wind waves. These experiments show that components of the wind waves with frequencies less than the frequency of the spectral peak (which is the portion of the spectrum that extracts energy from the wind) follow the linear dispersion relation. Phillips (1977) argues that the same should be true in the ocean.

The turbulent flow of the air over the water causes the dominant wave to be covered with ripples, i.e. waves of a wavelength that is much less than $L = 2\pi/k$, the wavelength

of the dominant wave. The effect of these ripples on the air flow is equivalent to an aerodynamic roughness, of length z_0, provided the Reynolds number, $z_0 u_*/\nu$, (u_* is the friction velocity of the air flow), is sufficiently large (in practice, greater than about 5).

A characteristic timescale of the evolution of the ripple field is the timescale for the growth of a ripple. Anticipating the results of §5.4, the growth of a wave of wavenumber k and period $T(k)$ occurs on a timescale

$$\tilde{T}(k) \sim \frac{\rho_w}{\rho_a}\frac{c^2}{u_*^2} T(k) \sim \frac{\rho_w}{\rho_a}\frac{c^2}{u_*^2}\frac{1}{ck}. \tag{2.5}$$

Hence longer waves grown on longer timescales. The laboratory experiments of Ramamonjiarisoa (1974) shows that all the ripples move with an approximately constant phase speed that is of the same order as the phase speed of the dominant wave. Hence, since the ripples have much shorter lengthscale, (2.5) shows that they grow on a timescale that is much shorter than that of the dominant wave. Because the flow is steady if the dominant wave does not grow, this suggests that the ripple field is in a local equilibrium where it responds to the local flow conditions. The waviness of the interface causes a variation along the wavelength in the flow properties and hence the ripple field. Effects that can cause a variation in the ripples include the variation of the air flow shear stress, advection by the orbital motions associated with the dominant wave and an associated instability (Longuet-Higgins & Stewart 1960), whereby ripples are steepened at the crest of the dominant wave.

Gent & Taylor (1976) showed that a variation in the roughness length along the wave may significantly effect the wave growth, but this effect has never been mathematically analysed and related to the other processes. In the present study, as a heuristic exercise, we focus on only the effects of the varying shear stress. The roughness length parameterizes the local drag force on the surface. Hence the roughness length is greatest where the concentration and steepness of the ripples is largest. The experiments of Wu (1979) suggest that the product of the number density and slope of the ripples is largest at the wave troughs. In §4.2.2 we show that this correlates with the shear-stress perturbation, $\Delta\tau^*$, induced by the wave interface, which is also largest at the crests. This suggests that the Charnock (1955) relation may be used to calculate the local change in roughness, Δz_0, from the local flow properties, since this implies that $\Delta z_0/z_0 = \Delta\tau^*/\rho_a u_*^2$. Other, more sophisticated, formulae could be used (e.g. that suggested by Wu 1968), but the scalings do not change and the added complexity does not seem justified. In §4.2.2 we describe how to calculate the perturbations to the air flow caused by this variation in roughness length.

When the roughness Reynolds number, $z_0 u_*/\nu$, is less than about 1, the ripples have little effect on the air flow and the surface is aerodynamically smooth. In this case the viscous sublayer may be represented by an equivalent roughness length $z_0 \approx 0.1\nu/u_*$. (This is justified because, as we show in §3.3, very close to the surface the perturbed air flow follows the classical law of the wall.)

In additon to the motions associated with the wavy interface, experiments (e.g. Wu 1975; Cheung & Street 1988) show that the mean shear stress of the wind induces a drift current in the water near the interface. The drift, of speed $U_d = O(u_*)$ at the surface, has both a kinematic and dynamic effect on the air flow. Its kinematic effect may be understood with the present theory, as is discussed briefly in §2.2. The recent numerical computations of the coupled air–water system by Harris (1992) suggest that the drift current does not have a significant dynamical effect on the growth of the slowly moving waves studied in this paper. The detailed dynamics of the drift current are therefore not considered in the present study.

2.2. *Flow in the air*

In the absence of the waves the air flow is statistically steady (at least on timescales long compared with a time for an eddy to be advected over a wavelength). The flow field is divided into a mean and turbulently fluctuating quantities. Near the surface, in the inner region, the unperturbed mean-flow profile $U_B(z)$ is assumed to vary logarithmically (even though the surface bounding the air flow is a liquid, laboratory experiments confirm this assumption, e.g. Hsu *et al.* 1981). Above the inner region the mean flow profile may take a more complex form, which makes it possible to apply the analysis to stratified flows in the environment. Initially we consider the problem in the frame in which there is no mean drift at the surface of the water so that $U_B(z_0) = 0$. In the frame of reference that moves with the wave crests, the unperturbed velocity profile becomes $\bar{U}_B = U_B - c$, where c is the wave phase speed. In cocurrent wind-wave flow $c > 0$, so that at the surface $\bar{U}_B < 0$. If $U_B(z)$ has a logarithmic profile, $\bar{U}_B$ is also logarithmic, i.e.

$$\bar{U}_B = (u_*/\kappa)\ln(z/z_m), \tag{2.6}$$

but z_0 is replaced by a different virtual origin $z_m = z_0 \exp(\kappa c/u_*)$, which is equal to the matched height, where the wind speed equals the wave speed. If there is a mean drift current in the water near the surface (of magnitude U_d at the interface), the mean velocity profile in the air is offset by a constant value, U_d, so that $\bar{U}_B = U_B - c + U_d$, i.e. the drift counteracts the effects of the non-zero wave speed and reduces the height of z_m. Hence this kinematic effect of the drift current is contained within the present analysis if, in the definition of z_m, c is interpreted as the wave speed minus the surface value of the drift current.

In the present study, we calculate the linear changes to the air flow caused by small-amplitude waves. The experimental data of Hsu *et al.* (1981) show that, for $ak = 0.107$, the linear perturbations to the air flow are within about 10% of the total perturbations. Furthermore, the nonlinear, numerical simulations of Gent & Taylor (1976) are also in acceptable agreement with linearized simulations for waves of small slope. Further evidence for the value of a linear calculation is provided by the success of the linear theory of flow over fixed topography (see e.g. Mason & King 1985, and BNH).

The wind feeds energy to the waves, which causes the wave amplitude to increase, and hence further modify the wind structure. In §5 we show that the rate of transfer of energy is proportional to (ρ_a/ρ_w), the ratio of the fluid densities ($\sim 10^{-3}$ for air over water) and the growth rate of the wave occurs on a timescale $O(T\rho_w/\rho_a)$, where T is the wave period. If L/U_0 is the time for a fluid element to be advected or distorted over one wavelength (U_0 is an advection speed that is defined more precisely below) then, since the wave shape is steady over a timescale long compared to L/U_0, the perturbations in the air are quasi-steady if $L/U_0 \ll T\rho_w/\rho_a$, which is always satisfied in practice for an air/water system. The steady solutions found here for the air flow are then valid up to times of $O(T\rho_w/\rho_a)$, and can be regarded as the leading-order term in a hierarchy of scaled time solutions analogous to those found by Janssen (1982) for the quasi-inviscid problem.

2.3. *Equations governing the air flow perturbations*

Non-dimensional forms of the mean velocities are defined with respect to the unperturbed value at a reference height h_m, so that $\bar{U}_B(z) = U_0 U(z)$, where $U_0 = \bar{U}_B(h_m)$. Later, h_m is defined to be the scale height of the middle layer where the leading-order pressure perturbation develops, so that the pressure scales on $\rho_a U_0^2$. The Reynolds stresses are made non-dimensional with the unperturbed surface shear stress, which is expressed as $\rho_a u_*^2$, where u_* is the unperturbed friction velocity.

The flow variables in the air are expressed as the unperturbed value for the flow in the absence of the wave plus a small perturbation: $u^* = U_B + \Delta u^*(x, z, t)$, etc. The wave slope is assumed small so that the perturbations are formally expanded in powers of ak, namely

$$\left.\begin{aligned} \Delta u^* &= U_0(aku^{[1]} + (ak)^2 u^{[2]} + \ldots), \quad \Delta w^* = U_0(akw^{[1]} + (ak)^2 w^{[2]} + \ldots), \\ \Delta p^* &= \rho_a U_0^2(akp^{[1]} + (ak)^2 p^{[2]} + \ldots), \quad \Delta\tau^*_{\alpha\beta} = \rho_a u_*^2(ak\tau^{[1]}_{\alpha\beta} + (ak)^2\tau^{[2]}_{\alpha\beta} + \ldots); \end{aligned}\right\} \tag{2.7}$$

$\Delta\tau^*_{\alpha\beta}$ is the Reynolds stress perturbation (for the shear stress $\tau^{[1]} \equiv \tau^{[1]}_{xz}$). These expansions are substituted into the Reynolds-averaged equations and successive terms are calculated iteratively. Only the solutions for the leading-order terms are calculated (so that the superscript [1] is omitted); the detailed analysis (HLR) shows that they are indeed proportional to ak.

Close to the surface the flow follows the undulation so that the presence of the undulating wave shape induces a vertical-velocity perturbation. To model this we introduce a (dimensionless) displaced coordinate system, (X, Z), which follows the surface close to the wave, i.e. $Z \sim kz - ak\,e^{ikx}$ as $kz \to ak\,e^{ikx}$, and tends to the Cartesian coordinates high above, i.e. $Z \sim kz$ as $kz \to \infty$. Hsu *et al.* (1981) discuss in detail the use of a displaced coordinate system. The form we use is similar to their suggestion (which follows from Benjamin 1959, and others); it is

$$kx = X - aki\,e^{iX}e^{-Z}, \quad kz = Z + ak\,e^{iX}e^{-Z}. \tag{2.8}$$

This smooth coordinate transformation is discussed in detail by Belcher (1990), see also BNH.

Flow perturbations expressed in the displaced coordinate system are denoted with subscript 'd'. On transforming to this system, the vertical-velocity perturbation, at leading order in ak, becomes,

$$\left.\begin{aligned} w(kz) &= i\,e^{iX-Z} + w_d(Z) \\ &\equiv w^{(0)} + w_d. \end{aligned}\right\} \tag{2.9}$$

The form of the transformation is chosen such that $w^{(0)}$ is the inviscid, irrotational flow induced by the undulation. The horizontal velocity perturbation in the displaced coordinate system is defined as being equal to that in the Cartesian coordinates, i.e. $u_d(Z) = u(kz)$.

The main effect of the coordinate transformation on the form of the governing equations is to provide a source term in the continuity equation which drives the perturbed flow, namely

$$\frac{\partial u_d}{\partial X} + \frac{\partial w_d}{\partial Z} = iUe^{-Z}. \tag{2.10}$$

In a frame moving with the wave crests, the equations governing the steady linear perturbations become

$$\left.\begin{aligned} U\frac{\partial u_d}{\partial X} + w_d\frac{dU}{dZ} &= -\frac{\partial p_d}{\partial X} + \epsilon^2\left(\frac{\partial \tau_d}{\partial Z} + \frac{\partial \tau_{XX}}{\partial X}\right), \\ U\frac{\partial w_d}{\partial X} &= -\frac{\partial p_d}{\partial Z} + \epsilon^2\left(\frac{\partial \tau_d}{\partial X} + \frac{\partial \tau_{ZZ}}{\partial Z}\right), \end{aligned}\right\} \tag{2.11}$$

where $\epsilon = u_*/U_0$ is a small parameter of the problem, which, for a stationary undulation, is typically 0.03–0.07 in the atmosphere. In §3.4, ϵ is related to $(u_* + c)/U_B(L)$, the basic small parameter of the problem. The Reynolds number is

assumed to be sufficiently large that either the flow is aerodynamically rough or that the flow very close to the surface follows the law of the wall (see §3.3); then the viscous stresses do not have to be considered explicitly. Equations (2.11) should each have two extra terms that arise from the coordinate transformation and involve the gradients of the unperturbed pressure and Reynolds stress distributions. In the very deep boundary layers considered here, these terms are numerically small and have been neglected (Belcher 1990).

Before discussing the boundary conditions to be imposed on (2.10) and (2.11), we observe that the moving wave induces two forcings on the air flow: the undulating shape of the wave, with perturbations denoted by superscript (U), and the non-zero value of the velocity at the surface of the wave, with perturbations denoted by superscript (S1). It is now shown that, for the linear perturbations, these two forcings may be analysed separately, so that the vertical-velocity perturbation may be written

$$w(kz) = w^{(0)}(Z) + w_{\mathrm{d}}^{(\mathrm{U})}(Z) + w_{\mathrm{d}}^{(\mathrm{S1})}(Z). \tag{2.12}$$

The (U)-perturbations arise mathematically from the source term in (2.10) that is a result of transforming to the displaced coordinates. Hence the (U)-perturbations are calculated from (2.10) and (2.11) with the boundary conditions

$$u_{\mathrm{d}}^{(\mathrm{U})}, w_{\mathrm{d}}^{(\mathrm{U})}, p_{\mathrm{d}}^{(\mathrm{U})}, \tau_{\mathrm{d}}^{(\mathrm{U})} \to 0 \quad \text{as} \quad Z \to \infty, \tag{2.13a}$$

$$u_{\mathrm{d}}^{(\mathrm{U})} = 0, \quad w_{\mathrm{d}}^{(\mathrm{U})} = 0 \quad \text{on} \quad Z = kz_0. \tag{2.13b}$$

The (S1)-perturbations are then needed to satisfy the non-zero surface velocity, which in the Cartesian coordinates are

$$u = \bar{u}\cos(kx), \quad w = \bar{w}\sin(kx) \quad \text{on} \quad z = \eta, \tag{2.14}$$

where, from (2.2), $\bar{u}^* = akU_0\bar{u}$ and $akc = \bar{w}U_0$. Evaluating (2.12) at the interface and using (2.13), (2.14) and $U_{\mathrm{B}}(z_0) = -c/U_0$, shows that

$$w_{\mathrm{d}}^{(\mathrm{S1})}(kz_0) = 0, \tag{2.15}$$

which is a consequence of the interface being steady and a streamline. Hence the (S1)-perturbations are calculated from the governing equations without the transformation-induced terms, i.e. equations (2.10) (with the right-hand side being zero) and (2.11), subject to the boundary conditions

$$u_{\mathrm{d}}^{(\mathrm{S1})}, w_{\mathrm{d}}^{(\mathrm{S1})}, p_{\mathrm{d}}^{(\mathrm{S1})}, \tau_{\mathrm{d}}^{(\mathrm{S1})} \to 0 \quad \text{as} \quad Z \to \infty, \tag{2.16a}$$

$$u_{\mathrm{d}}^{(\mathrm{S1})} = \bar{u}\cos X, \quad w_{\mathrm{d}}^{(\mathrm{S1})} = 0 \quad \text{on} \quad Z = kz_0, \tag{2.16b}$$

i.e. flow over a flat rubber sheet carrying longitudinal waves!

3. Asymptotic structure of the perturbations

In this section the asymptotic structure of the linear perturbations is discussed. HLR found that the perturbations to a turbulent boundary layer passing over a low hill could be analysed within a four-layer structure, and BNH show that this structure is capable of describing a whole class of perturbations to turbulent boundary-layer flows. An important difference in the moving-wave problem is that, in the frame moving with the wave crests, the unperturbed velocity profile has a region of reversed flow below z_{m} which does not appear when the obstacle is fixed (i.e. a hill). In this study, we restrict attention to small values of $(u_* + c)/U_{\mathrm{B}}(L)$ so that the region of reversed flow is very thin. It is assumed, and justified *a posteriori*, that in the limit of $(u_* + c)/U_{\mathrm{B}}(L) \ll 1$, the same four-layer structure describes the flow. A new solution is required for the

perturbations in the thin region of reversed flow and at the matched height. The analysis shows that this layer has only a small effect on the perturbed flow above. In §3.4 we examine the restrictions placed on the validity of the solutions by the assumption that the HLR four-layer structure describes the perturbations.

3.1. *Changes to the turbulence structure*

Define a Lagrangian timescale of the turbulence, e.g. an eddy turnover time

$$T_{\mathrm{L}}(Z^*) = Z^*/u_* \text{ (where } Z^* = Z/k).$$

Also, let

$$T_{\mathrm{D}}(Z^*) = k^{-1}/U(Z^*) = k^{-1}/\{(u_*/\kappa)\ln(Z^*/z_{\mathrm{m}})\}$$

be the timescale for an eddy to be advected and distorted over the wave. Then $T_{\mathrm{L}} \sim T_{\mathrm{D}}$ when $Z^* \sim l$, $kl\ln(l/z_{\mathrm{m}}) \sim 1$, and it is convenient to fix the constant so that

$$kl\ln(l/z_{\mathrm{m}}) = 2\kappa^2. \tag{3.1}$$

The flow is consequently divided into two regions: the inner region, where $Z = O(kl)$, and the outer region, where $Z = O(1)$. Towards the surface where $Z/kl \to 0$, $T_{\mathrm{L}} \ll T_{\mathrm{D}}$ and the turbulence tends to a local equilibrium. In the outer region, where $Z \gg kl$, $T_{\mathrm{D}} \ll T_{\mathrm{L}}$ and the changes to the turbulence are 'rapid', i.e. dependent on the history of the strain, and not on the local velocity gradient.

This argument shows that, as the surface is approached, since the turbulence is in local equilibrium, it is dependent on only the local gradient of the mean velocity. BNH discuss the effects of curvature, and advection and diffusion of turbulent energy, which are also important when $Z \sim kl$. They show that the effects on the mean flow are small. For the present purposes, the main conclusion from BNH is that the Reynolds shear stress can be modelled adequately by a perturbation mixing-length formula (Townsend 1965) throughout the inner region, viz.

$$\tau_{\mathrm{d}} = \frac{2\kappa}{\epsilon} Z \frac{\partial u_{\mathrm{d}}}{\partial Z}. \tag{3.2}$$

Furthermore, the linear changes to the normal Reynolds stresses in the inner region are proportional to the changes to the shear stress, so that

$$\tau_{XX} = -\alpha\tau_{\mathrm{d}}, \quad \tau_{ZZ} = -\beta\tau_{\mathrm{d}}, \tag{3.3}$$

where the constants α and β are determined from measurements of an equilibrium atmospheric boundary layer, taken here as $\alpha = 6.3$, $\beta = 1.7$ (a fuller discussion of this approximation can be found in BNH).

The analysis of the timescales also shows that in the outer region the distortion of the turbulence is 'rapid', so is determined by the history of the straining of the eddies, and not on the local gradient of mean velocity, or the interaction with the other eddies. The changes to the normal Reynolds stresses may then be expanded in power series of the velocity perturbation, e.g.

$$\frac{\Delta\tau_{\mathrm{d}}^*}{\rho_{\mathrm{a}} u_*^2} = \frac{\Delta u_{\mathrm{d}}^*}{U_0} C_1 + \left(\frac{\Delta u_{\mathrm{d}}^*}{U_0}\right)^2 C_2 + \ldots \tag{3.4}$$

(Britter, Hunt & Richards 1981). This shows that in the outer region $\Delta(\tau_{\mathrm{d}}^*)_{ij} = O(aku_*^2)$. The dimensionless Reynolds-stress gradients are then of $O(1)$, which, through the mean momentum equation (2.11), produces dimensionless velocity perturbations that are of $O(\epsilon^2)$. If the mixing-length model is erroneously used in the outer region, $\Delta\tau_{\mathrm{d}}^*$ is of

$O(akU_0 u_*)$, which leads to dimensionless velocity perturbations that are too large by a factor of $O(1/\epsilon)$; this leads to significantly different values for the wave growth rate, see §5.5.

3.2. *Structure of the mean flow perturbations*

We now examine the structure of the linear changes to the mean flow when the boundary layer is subjected to a linear forcing. The unperturbed velocity profile is written

$$U(z) = (\epsilon/\kappa)\ln(z/z_m), \tag{3.5}$$

then the scaling arguments of BNH can be used with z_m replacing z_0.

As shown in §3.1 above, in the outer region the leading-order perturbations are described by inviscid dynamics, because the Reynolds stress gradients are $O(\epsilon^2)$ smaller than the inertial gradients, and (2.11) can be reduced to a single equation for the vertical velocity perturbation,

$$\frac{\partial^2 w_d}{\partial X^2} + \frac{\partial^2 w_d}{\partial Z^2} - \frac{U''}{U} w_d = O(\epsilon^2). \tag{3.6}$$

Asymptotic solutions to this equation may be found by separating the outer region into two layers: an upper layer, $Z = O(1)$, where the shear in the unperturbed profile is assumed small compared with the streamwise variations ($\partial^2 w_d/\partial X^2$); and a middle layer, $Z = O(kh_m)$, where the shear is larger than the horizontal variations. The scale height, h_m, of the middle layer is the height at which these two processes balance, i.e.

$$\partial^2 w_d/\partial X^2 \sim U'' w_d/U; \tag{3.7}$$

so that if U is a logarithmic profile,

$$kh_m \ln^{\frac{1}{2}}(h_m/z_m) = 1. \tag{3.8}$$

The scale for the velocity perturbations, U_0, is then defined to be $\bar{U}(h_m)$. The solutions in the outer region are found iteratively as power series in $kh_m = (\epsilon/\kappa)^{\frac{1}{2}}$.

Throughout the bulk of the inner region, in the shear stress layer (referred to as the SSL), where $Z = O(kl)$, the perturbation pressure gradient balances the inertial term at zeroth order. The shear-stress gradient balances the difference of these terms at first order in the small parameter δ, where

$$\delta = \ln^{-1}(l/z_m) = \epsilon/\kappa U(l) = O(\epsilon). \tag{3.9a}$$

The dimensionless value of the unperturbed velocity $U(l) = 1 + O(\delta \ln(1/\delta))$. The asymptotic solution in the SSL is calculated in terms of $\zeta = Z/kl = O(1)$, with the dependent variables scaled as

$$u_d = \frac{\hat{u}_d}{U(l)} e^{iX}, \quad w_d = \frac{\hat{w}_d}{U(l)} e^{iX}, \quad \tau_d = \frac{2\hat{\tau}_d}{U^2(l)} e^{iX}, \quad p_d = -\hat{p}_d e^{iX}. \tag{3.9b}$$

Substituting for the unperturbed velocity profile, and using the mixing-length formula for the shear and normal stress, the X-momentum equation becomes

$$\frac{\partial}{\partial\zeta}\left(\zeta\frac{\partial\hat{u}_d}{\partial\zeta}\right) - i\hat{u}_d = -i\hat{p}_d + \frac{\hat{w}_d}{2\kappa^2\zeta} + \delta i\hat{u}_d \ln\zeta - \delta 2i\kappa^2\alpha\zeta\frac{\partial\hat{u}_d}{\partial\zeta}. \tag{3.10a}$$

The scaled perturbations are expanded in powers of δ, and the solutions found iteratively (HLR). The first two terms in the solution for $\hat{u}_d$ are

$$\hat{u}_d = -\hat{\sigma}^{(0)}\{1 + \delta(1 - \ln\zeta - 4K_0[2(i\zeta)^{\frac{1}{2}}])\}, \tag{3.10b}$$

where $\hat{\sigma}^{(0)} = -1$ is the leading-order solution for the scaled-pressure perturbation at the surface and K_0 is the modified Bessel function (Abramowitz & Stegun 1972). The significance of this result is that $K_0[2(\mathrm{i}\zeta)^{\frac{1}{2}}]$ has real and imaginary parts, so that $\hat{u}_d$ is asymmetric with respect to the wave elevation. Furthermore, (3.10*b*) shows that the streamwise velocity perturbation has the asymptotic forms $\Delta u \sim -\ln\zeta$ as $\zeta \to \infty$ and $\Delta u \sim \ln\zeta$ as $\zeta \to 0$. Hence there is a maximum in the velocity perturbation within the inner region.

The solution for the shear-stress gradient found using this technique, diverges logarithmically as the surface is approached, Sykes (1980). The shear-stress gradient adjusts to the finite surface value across a very thin layer close to the surface (the inner surface layer referred to as the ISL), which is considered in the next section.

3.3. *Analysis of the inner surface layer and the matched height*

The pioneering work of Miles (1957) attached considerable importance to the matched height in the wind generation of waves. In this section we show that, for the slow waves considered in this study, the matched height lies within the (ISL) and does not have a dynamical effect on the perturbed flow.

The solution (calculated from (3.10) and (3.2)) for the shear-stress gradient in the SSL shows that

$$\partial\tau_d/\partial\zeta \propto \delta \ln\zeta \quad \text{as} \quad \zeta \to 0, \tag{3.11}$$

i.e. it diverges logarithmically towards the surface. The exact (and finite) surface boundary condition for $\partial\tau_d/\partial Z$ may be constructed from the X-momentum equation (see (3.13*c*) below). Asymptotically correct solutions for the perturbations are obtained by analysing an even thinner layer, the ISL, which is exponentially thin compared with the SSL. In the ISL $Z = O(kz_m)$ so that the matched height lies within this layer. A practical estimate for the depth of the ISL, l_s, is the height where the shear-stress gradient calculated from the SSL solution equals the exact, surface value. This implies that

$$l_s = (lz_m)^{\frac{1}{2}}. \tag{3.12}$$

The ISL is most easily analysed in terms of the perturbation shear stress, τ_d, which changes very little across this layer. Eliminating the pressure terms between the X- and Z-momentum equations, and then using the continuity equation and mixing-length formula, (3.10*a*) reduces to an equation for $\hat{\tau}_d$, namely

$$\frac{\partial^2\hat{\tau}_d}{\partial\eta^2} = kz_m \frac{\mathrm{i}}{2\kappa^2\eta}\left[\hat{\tau}_d \ln\eta + \langle\hat{\tau}_d\rangle + \frac{2\kappa}{\epsilon}\frac{\eta}{\eta_0}\bar{u}\right] + O((kz_m)^2), \tag{3.13a}$$

where $\eta = Z/kz_m$, the hatted variables are defined in (3.9*b*), and

$$\langle\hat{\tau}_d\rangle = \int_{\eta_0}^{\eta} \hat{\tau}_d(\eta')\left[\frac{1}{\eta} - \frac{1}{\eta'}\right]\mathrm{d}\eta', \tag{3.13b}$$

where $\eta_0 = z_0/z_m$. A boundary condition on the shear-stress gradient may be constructed by considering the X-momentum equation at the wave surface, where $u_d(\eta_0) = \bar{u}$, $w_d(\eta_0) = 0$, $U(z_0) = -c/U_0$, and $p_d(\eta_0) = \hat{\sigma}$, so that

$$2\kappa^2\delta^2 \frac{\partial\hat{\tau}_d}{\partial\eta}\bigg|_{\eta_0} = \mathrm{i}kz_m\left[\hat{\sigma} - \frac{c}{U_0}\bar{u}\right]. \tag{3.13c}$$

Solutions to (3.13) are calculated iteratively by expanding the perturbations in

powers of kz_m and then in δ. Providing $kz_m|\ln(z_m/z_0) \ll 1$ (a condition which is examined in §3.4 below) then at $O([kz_m]^0)$,

$$\partial\hat{\tau}_d^{(0)}/\partial\eta = 0. \tag{3.11a}$$

Hence at leading order the shear stress across the ISL is constant,

$$\hat{\tau}_d^{(0)} = \hat{\tau}_d^{(0)}(\eta_0), \tag{3.14b}$$

and is determined by matching with the SSL solutions. Furthermore, using the mixing-length formula, the velocity perturbation is calculated as

$$\hat{u}_d^{(0)} = \delta\hat{\tau}_d^{(0)}(\eta_0)\ln\eta. \tag{3.14c}$$

At $O(kz_m)$, (3.13a) can be integrated to give

$$\frac{\partial\hat{\tau}_d^{(1)}}{\partial\eta} = \frac{\partial\hat{\tau}_d^{(1)}}{\partial\eta}\bigg|_{\eta_0} + \frac{i}{2\kappa^2}\left[\hat{\tau}_d^{(0)}(\eta_0)\left(\frac{\eta_0}{\eta} + \ln(\eta/\eta_0)(1+\ln\eta_0)\right) + \frac{U(l)}{\delta}\bar{u}\eta_0\ln(\eta/\eta_0)\right], \tag{3.15}$$

where $\partial\hat{\tau}_d^{(1)}/\partial\eta|_{\eta_0}$ is determined from (3.13c). These solutions show that the shear-stress gradient is non-singular at the matched height, when $\eta = 1$. The matched height therefore plays no significant dynamical role in the flow for the small wave speeds considered here.

In the ISL, τ_d and $\partial\tau_d/\partial\eta$ are the slowly varying quantities, so that approximate solutions can be constructed by considering the equation for the shear stress. This approach avoids the apparent singularity in the momentum equation at z_m, where the unperturbed velocity has a zero. The key feature is that, although $U \sim 0$ near the matched height (so that $u_d(Z)$ may not remain small compared to $U(Z)$), the velocity and shear stress perturbations remain small compared to $U_B(l)$ and u_*^2 respectively. The equation for the turbulent shear stress shows that it remains appropriate to expand the perturbations as power series in the wave slope. It is therefore inappropriate to apply the inviscid, Miles (1957) theory to the slowly moving waves considered here. (Miles 1967 recognized that the Reynolds stresses play a significant role in the wave growth.)

3.4. *Range of wave speeds for the asymptotic analysis to be valid*

The solutions are valid when $\delta \ll 1$, i.e. when

$$1 + \ln(z_m/z_0) \ll \ln(l/z_0) \tag{3.16a}$$

but we have the relations $\ln(z_m/z_0) = \kappa c/u_*$, and $\ln(l/z_0) \sim U_B(l)/u_* \sim U_B(L)/u_*$, so that the condition for the analysis to be valid, equation (3.16a), may be written

$$(u_* + c)/U_B(L) \ll 1. \tag{3.16b}$$

In fact this condition is equivalent to $\epsilon = u_*/U_0 \ll 1$, since

$$U_0 = \bar{U}_B(h_m) = U_B(h_m) - c \sim U_B(L) - c, \tag{3.17}$$

so that

$$\epsilon = \frac{u_*}{U_0} \sim \frac{u_* + c}{U_B(L)}\left[1 + O\left(\left[\frac{c}{U_B(L)}\right]^2\right)\right]. \tag{3.18}$$

The shear stress in the ISL is constant at leading order provided $kz_m\ln(z_m/z_0) \ll 1$.

This condition is always satisfied when c is positive and (3.16) is satisfied: $kz_m = O(\delta e^{-1/\delta})$, so that

$$kz_m \ln(z_m/z_0) \sim \delta e^{-1/\delta} \frac{1}{\delta} \frac{\kappa c}{U_0} \ll \frac{\kappa c}{U_0} \ll 1. \tag{3.19}$$

When c is negative (for countercurrent wind/wave flow) $|kz_m \ln(z_m/z_0)| \ll 1$ if

$$|u_* + c|/U_0 \ll 1. \tag{3.20}$$

4. Characteristics of the perturbed flow

In a frame moving with the wave crests, the wave is steady and produces two forcings on the boundary layer above, namely (i) the undulating shape of the wave, with perturbations denoted by superscript (U), and (ii) the non-zero varying tangential velocity at the surface, with perturbations denoted by superscript (S1). For a linear analysis of small perturbations, the effects of these two forcings can be analysed separately. We also consider the effect of a varying surface roughness, with perturbations denoted by superscript (S2).

The solutions for the perturbations induced by each of the forcings are quoted from the previous studies of HLR, BNH and Belcher, Xu & Hunt (1990). In order to understand the processes that govern the growth of the wave, it is necessary to review some aspects of these solutions.

4.1. *Perturbations forced by the undulation*

In §2.3, the perturbations to the flow over the undulating wave shape were shown to be forced by a vertical-velocity perturbation induced by the surface. The unperturbed velocity profile has a region of reversed flow below the matched height. In the ISL this leads to differences between the perturbations induced by moving and rigid undulations (see §3.3). Above the ISL the movement of the wave has the kinematic effect of changing the virtual origin of unperturbed velocity to z_m and thence modifying the scale heights of the asymptotic layers. Otherwise the analysis of the layers above the ISL follows HLR and BNH; these solutions are listed in Appendix A. This component of the solution is denoted by superscript (U). The perturbations have been scaled so that $u_d^{(U)} = O(1)$, i.e. the undulation induces $\Delta u^* = O(akU_0)$.

A key feature of these solutions is that, as explained in §3.2, within the SSL the balance in (3.10*a*) at $O(\delta)$ the Reynolds shear stress and inertial terms leads to the streamwise velocity perturbation, $u_d^{(U)}$, being smaller by $O(\delta)$ on the downwind slope than on the upwind slope, i.e. it is out of phase with the potential flow solution (see figure 2*b*, which shows only streamlines above the recirculating region). BNH examined the implications of this asymmetry and showed that continuity implies that $w_d^{(U)}$ has an asymmetrical component of $O(\delta^2)$ and the associated asymmetrical vertical and horizontal pressure gradients are also of $O(\delta^2)$. An alternative explanation for this asymmetric pressure perturbation is that the asymmetry of the streamlines in the (SSL) causes the potential flow in the upper layer is displaced slightly out of phase with the wave surface. This was termed *non-separated sheltering* by BNH.

The pressure perturbation that is in phase with the wave slope plays a central role in the mechanism of the growth of the wave. BNH make a careful study of the various processes that can induce an asymmetric pressure at the surface of a fixed undulation (the mechanisms designated NSS, IRS, ORS and FAD in §1 and see figures 2–8) and

show that non-separated sheltering leads to the dominant contribution, the other effects being a factor of $O(\delta)$ smaller. The arguments leading to these conclusions do not involve analysing the ISL, hence, since in the present moving-wave problem the flow perturbations above the ISL are equivalent to those induced by a fixed undulation with an unperturbed velocity profile that has a virtual origin at z_m (see §3.2), the same conclusions hold in the present flow. Furthermore, BNH calculate the asymmetric pressure perturbation using linear theory and thence the contribution to the drag arising from non-separated sheltering. The resulting formula for the drag is in excellent agreement with values computed using the complete, nonlinear, Reynolds-averaged, momentum equations using a second-order closure model for the turbulent stresses (see BNH figure 11).

The essential feature of this linear model is that the mixing-length model for the shear stress perturbation is used in the inner region only; the perturbations to the Reynolds stress components in the outer region are determined by the rapid distortion mechanism (see §3.1). If the mixing-length formula is erroneously used throughout the perturbed flow then the calculated asymmetric pressure perturbation is too large by $O(1/\epsilon)$, which leads to overly large estimates of the drag (see BNH figure 11; figure 10 below) and the energy flux to the wave motion (see §5).

4.2. *Perturbations induced by the surface boundary conditions*

4.2.1. *Perturbations forced by the orbital velocity at the wave surface*

Now consider the component of the perturbations induced by the orbital velocity of the water at the surface of the wave, which is denoted by superscript (S1).

Formally the solution for varying surface velocity is the same (except in the ISL) as caused by a change in the surface roughness length from z_0 to $z_0+\Delta z_0$: a change of velocity at a given height z_0 is equivalent (at a height much greater than z_0) to changing the height, from z_0 to $z_0+\Delta z_0$, at which the velocity is zero. The perturbations induced by a varying surface roughness have been analysed by Belcher, Xu & Hunt (1990) using the same analytic framework of inner and outer regions as for fixed undulations (similar results were also obtained by Walmsey, Taylor & Keith 1986). When the roughness length of the surface changes to $z_0+\Delta z_0$, the perturbation velocity at a height z_0, to first order, is

$$\Delta u^*(z_0) = -(u_*/\kappa)\ln(1+\Delta z_0/z_0). \tag{4.1}$$

Conversely, if $u^*(z_0)$ is changed by Δu^*, the equivalent change in roughness length is given by

$$z_0+\Delta z_0 = z_0\exp(-\kappa\Delta u^*/u_*). \tag{4.2}$$

Hence, the solutions of Belcher *et al.* (1990) for the perturbations due to a varying surface roughness can be modified and used to calculate the perturbations induced by the varying surface velocity. In Appendix B we list these solutions in the form which satisfies a varying tangential surface velocity.

From (2.16*b*), the tangential velocity induced by the orbital motions at the surface is, $u_d^{(S1)}(kz_0) = \bar{u}\cos X$; for deep-water gravity waves, this becomes

$$u_d^{(S1)}(kz_0) = (c/U_0)\cos X = U(l)\,\delta\ln(z_m/z_0)\cos X. \tag{4.3}$$

Our theory is valid when $\ln(z_m/z_0) = O(1)$ (see §3.4), so that the (S1)-perturbations are smaller by $O(\delta)$ than the (U)-perturbations, which are $O(1)$ (see §4.1).

The streamlines of the perturbations due to varying tangential velocity are sketched in figure 7. The variation in the surface velocity accelerates and decelerates the flow in

phase with the surface variations near to the surface, in the lower part of the inner region. The orbital motion of the water at the surface of the wave is in phase with the elevation of the surface, and hence, close to the surface, the streamwise velocity in the air is also in phase with the wave displacement. By contrast, at the top of the inner region, the interaction between the inertial- and shear-stress perturbations leads to the acceleration and deceleration of the flow being out of phase with the surface elevation. Continuity then leads to a second-order vertical velocity which drives the outer-region flow and leads to a streamwise $u^{(S1)}$ (and hence a $p^{(S1)}$) perturbation in the upper layer which is in anti-phase with the wave slope. Hence, the boundary layer tends to be thinned downwind of the wave crest, in contrast to the direct effect of the undulating wave shape which thickens the boundary layer in the lee of the crest. A more complete discussion of this phase shift is given in Belcher *et al.* (1990). The solutions (B 2) and (B 4) in Appendix B show that the asymmetric pressure perturbation induced by the orbital surface velocity is

$$p_{\mathrm{d}}^{(S1)} = O(-(ak)\,\delta^3 \ln(z_{\mathrm{m}}/z_0)),$$

i.e. $O(\delta \ln(z_{\mathrm{m}}/z_0))$ smaller than the asymmetric part of $p_{\mathrm{d}}^{(U)}$.

4.2.2. *Perturbations due to the varying surface roughness*

By linearity, the variation of the surface roughness may be accounted for by calculating perturbations due to a flat surface with varying surface roughness and adding them to the other two components of the solution. The component of the solution induced by the change of roughness is denoted by superscript (S2).

The local change in the roughness length is assumed, following Charnock (1955), to be proportional to the local change in the shear stress (see §2.1 for a full discussion). The solutions in the Appendices show that the undulations and the orbital surface velocity induce variations in the shear stress at the surface of the wave of magnitudes $\Delta\tau_{\mathrm{d}}^{*(U)}(kz_0) = O(aku_*^2)$ and $\Delta\tau_{\mathrm{d}}^{*(S1)}(kz_0) = O(aku_*^2\,\delta \ln(z_{\mathrm{m}}/z_0))$ respectively. Hence, at leading order, the surface shear-stress perturbation is induced by the undulating wave shape and so produces the dominant change to the surface roughness:

$$\frac{\Delta z_0}{z_0} = \frac{\Delta\tau^{*(U)}}{\rho_{\mathrm{a}} u_*^2} = ak\frac{2}{U^2(l)}\cos X + O(ak\delta), \tag{4.4}$$

and the surface roughness is increased at the wave crests (where the perturbed shear stress is maximum) and decreased at the troughs.

The effective tangential surface velocity is

$$\Delta u^{*(S2)}(z_0) = -\frac{u_*}{\kappa}\ln\left[1+\frac{\Delta z_0}{z_0}\right] = -\frac{u_*}{\kappa}\left[ak\frac{2}{U^2(l)}\cos X + O(ak\delta, (ak)^2)\right], \tag{4.5}$$

so that the flow is decelerated at the crest, contrary to the effect of the orbital velocity, which accelerates the boundary layer at the crest. The variation in the surface roughness, like the presence of the undulation, tends to thicken the boundary layer on the leeside of the wave. The combined effect of the variations of surface roughness and orbital velocity can then be viewed as providing an overall tangential surface velocity,

$$u_{\mathrm{d}}^{(S1)+(S2)}(kz_0) = \delta U(l)[\ln(z_{\mathrm{m}}/z_0) - 2/U^2(l)]\cos X, \tag{4.6}$$

and these two effects balance when

$$\kappa c/u_* \equiv \ln(z_{\mathrm{m}}/z_0) = 2/U^2(l). \tag{4.7}$$

For wave speeds greater than this critical value, the perturbed boundary layer is thinner on the leeside of the crest than for the equivalent rigid undulation. In many practical situations, the flow is such that these two effects are close to cancelling.

4.3. *Discussion of the complete solution*

What are the similarities and differences between the solutions derived for a fixed undulation and the moving wave? The leading-order mean-velocity perturbations due to the undulations are $u_d^{(U)} = O(1)$. The varying tangential velocity of the (S1) perturbations is $O(\delta \ln(z_m/z_0))$, and the effective tangential velocity of the (S2) perturbations is $O(\delta)$. Furthermore, the perturbations induced by a varying tangential velocity (Appendix B) are rather small: in the SSL, $u_d^{(S1)}$ is a factor of $O(\delta)$ smaller than the surface value. So that, overall, the velocity perturbations due to the surface effects in the SSL and above are of $O(\delta^2)$ smaller than the undulation-induced perturbations. The unperturbed velocity for the moving wave is different from the static case, which leads to terms proportional to $\ln(z_m/z_0)$ in the three components of the inner-region solutions that are absent when the undulation is static. These extra terms, however, are also of $O(\delta^2)$. These arguments show that formal differences between the solutions for the velocity perturbations over a moving wave and over the equivalent fixed rigid undulation are of $O(\delta^2)$.

There is, however, a more subtle dependence on the relative wave speed: the scaling arguments of §3 were performed using $U(z) = (\epsilon/\kappa)\ln(z/z_m)$. The dominant effect of the motion of the wave on the solutions in the SSL and outer region is then this kinematic effect of changing the virtual origin of the unperturbed velocity profile from z_0 to z_m. The perturbed flow is thus the same as over a fixed rigid wave, of the same wavelength, with its surface at $Z = kz_m$; the corrections are of $O(\delta^2)$ only.

Despite the similarity of the gross features of the mean flow to those of a fixed undulation, it is precisely the subtle, second-order, asymmetric effects which are important in determining the growth of the wave, §5, and increased drag force on the wave, §6. In particular, the combined effects of (S1) and (S2) either add to or subtract from the asymmetric parts of the flow, as discussed in §4.2.2. The small $O(\delta \ln(z_m/z_0))$ effect of the orbital velocity increases with $\ln(z_m/z_0)$, and can decrease the asymmetry of the perturbed boundary layer induced by the (U) perturbation.

We now examine the profiles of the mean velocity and shear-stress perturbations and compare with the experimental data of Hsu *et al.* (1981). For this experiment the parameters are $k = 0.04\ \mathrm{cm}^{-1}$, $a = 2.67$ cm, so that $ak = 0.107$, $u_* = 8.5\ \mathrm{cm\ s}^{-1}$ and $c = 156\ \mathrm{cm\ s}^{-1}$. Hsu *et al.* show that the unperturbed velocity profile matches a logarithmic profile only very close to the surface (presumably this is an artifact of the relatively low Reynolds number of their experiment). Hence in determining the matched height, which is $z_m = 0.8$ cm, and the scale heights of the asymptotic layers we have used the unperturbed velocity profile they suggest (their equation (4.5) and figure 3). This leads to $l = 7$ cm and $h_m = 15$ cm, so that the small parameters for the theory are $\delta = 0.5$ and $kh_m = 0.6$. These parameters are clearly not small, so that any comparisons can be only qualitative (we found very few data sets of velocity and shear-stress measurements in the literature, the Hsu *et al.* data coming closest to meeting the requirements of the theory).

Figure 9 shows the profile of the mean velocity perturbation at the crest of the wave. The data were obtained from Hsu *et al.*'s figure 5. The large value of δ is reflected in the large near-surface perturbations associated with the (S1) and (S2) effects. Although the profiles do not agree too well, the magnitude of the maximum velocity perturbation is well captured by the (U)-perturbations. The discrepancy between the theory and the

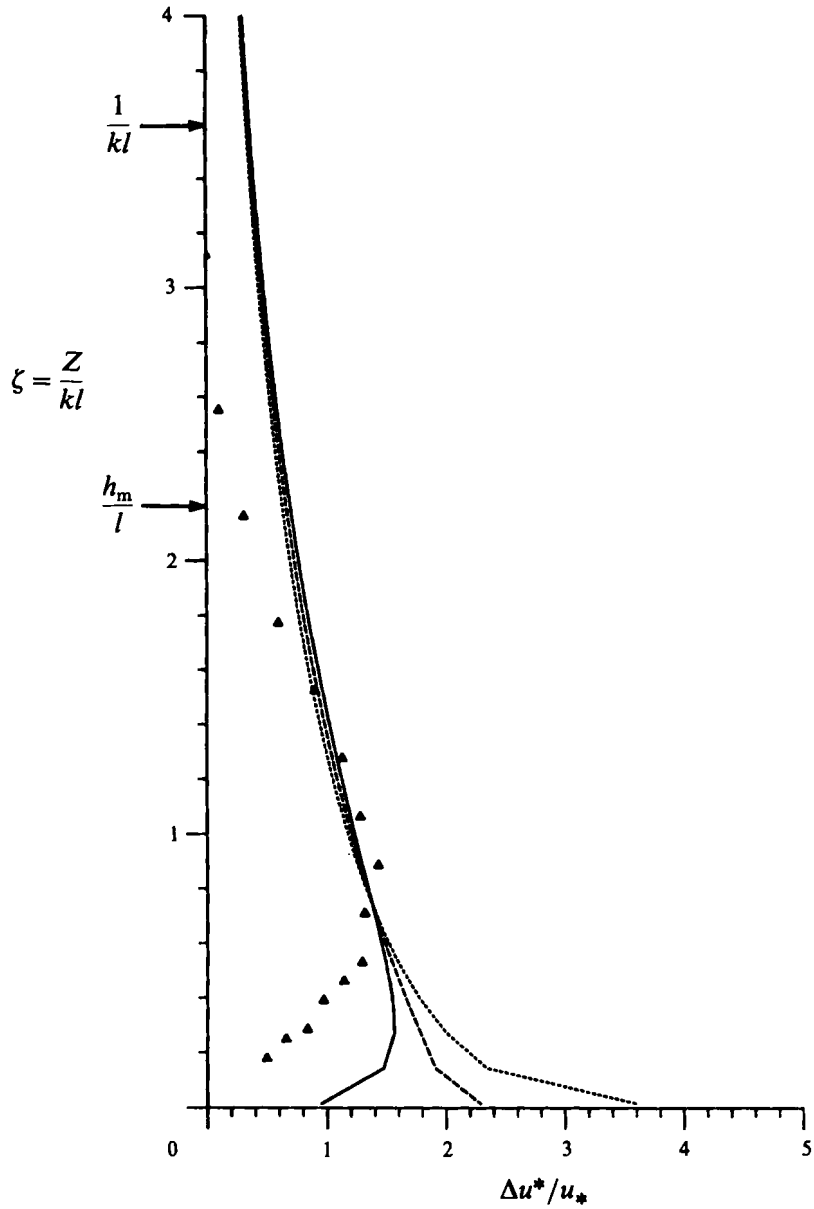

FIGURE 9. Velocity perturbation, calculated using the linear theory, at the crest of a sinusoidal wave and comparison with the data of Hsu *et al.* (1981). $ak = 0.107$; $c = 156$ cm s^{-1}; $u_* = 8.5$ cm s^{-1}; $z_m = 0.8$ cm. ——, (U) solution; ....., (U)+(S1) solution; – – –, (U)+(S1)+(S2) solution; △, measurements of Hsu *et al.* (1981).

data at higher levels is perplexing: the theory shows an exponential decay of the perturbations on the $Z = O(1)$ lengthscale, whereas the data decay much more rapidly. Field measurements of the pressure perturbation above a wave field (e.g. Snyder *et al.* 1981) have reported an $e^{-Z} \sim e^{-kz}$ decay at large heights; one would then expect a similar decay of the velocity perturbation. A second perplexing aspect of the Hsu *et al.* data is that the perturbations appear to be falling to zero at the wave surface. At the crest of the wave, according to irrotational theory, the orbital motions of the wave motion are maximum, which leads to the large increase in the theoretical values of the

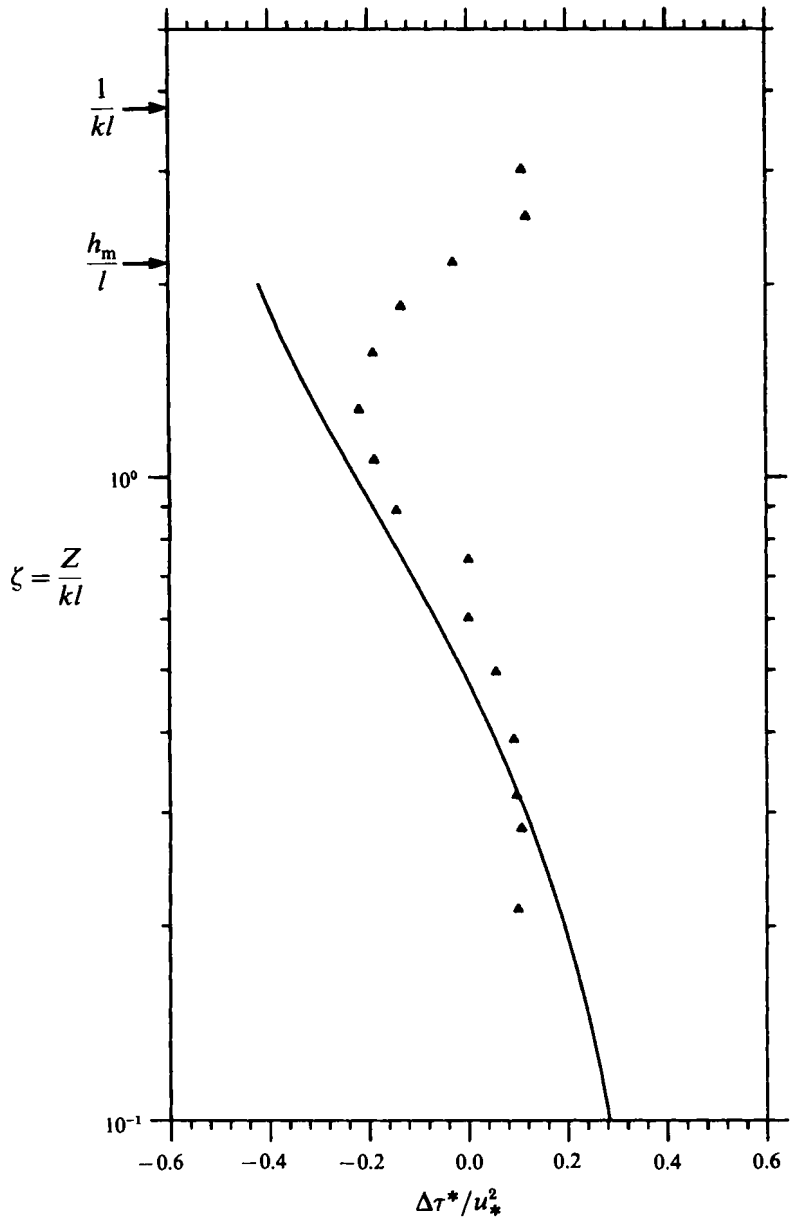

FIGURE 10. Profile of the shear stress at the crest of a sinusoidal wave from the theory and from the measurements of Hsu *et al.* (1981). Note the limited range of validity of the theoretical curve. Same parameters as figure 9. ——, (U) solution; △, measurements of Hsu *et al.* (1981).

velocity near the surface (dotted line): perhaps the Hsu *et al.* data give an indication that the irrotational-wave theory is inappropriate. In view of the large value of δ it is hard to draw strong conclusions.

Figure 10 shows the profile of the shear-stress perturbation at the crest of the wave. The data were obtained from Hsu *et al.*'s figure 10, which gives $-\Delta\tau^*$. In view of the mean velocity in Hsu *et al.*'s data going to zero at the surface, we plot only the (U)-perturbation component. Despite the large value of δ, the agreement between the theory and data is reasonable both qualitatively and quantitatively. The theoretical

curve has been truncated at $\zeta = 2$; the large δ-value means that this is similar to the scale height of the middle layer. Notice how the data show that the shear-stress perturbation is small and positive in the outer region. If the mixing-length model were used here, the shear-stress perturbation would be large and negative! By truncating the mixing-length model above the inner region, we avoid this qualitative discrepancy (see also BNH). The agreement between the theory and data for the shear stress is important. BNH show that the pressure perturbation, $\mathrm{Im}\,(p_\mathrm{d})$, that is in phase with the wave slope is related to the shear-stress perturbation that is in phase with the wave elevation, $\mathrm{Re}\,(\tau_\mathrm{d})$, which is plotted in figure 10. Hence according to BNH

$$\mathrm{Im}\,(p_\mathrm{d}) = \mathrm{i}\frac{\epsilon^2}{U^2(l)}\mathrm{Re}\,[\tau_\mathrm{d}(\zeta\to\infty)-\tau_\mathrm{d}(0)].$$

We therefore expect that the theory should give reliable estimates for the growth of the wave (which is strongly dependent on $\mathrm{Im}\,(p_\mathrm{d})$, §5).

We also compared our theoretical mean-velocity perturbations with the profiles computed by Gent & Taylor (1976). We found that the profiles were in qualitative disagreement and are not shown here. We note that Hsu *et al.* (1981) also found serious discrepancies between their data and the values computed by Gent & Taylor (1976).

5. Liquid motions and the growth rate of the wave

The equation for the energy of the perturbed motions in the water (expressed in the Cartesian coordinate system and in a frame moving with the wave crests) is

$$\Delta u_i^*\frac{\partial \Delta u_i^*}{\partial t}+\Delta u_i^* U_j\frac{\partial \Delta u_i^*}{\partial x_j}+\Delta u_i^*\Delta u_j^*\frac{\partial U_i}{\partial x_j}=\frac{1}{\rho_\mathrm{w}}\Delta u_i^*\frac{\partial \Delta\sigma_{ij}^*}{\partial x_j}-g'\frac{\partial \eta}{\partial x_i}\Delta u_i^*, \tag{5.1}$$

where $\Delta\sigma_{ij}^*$ is the perturbation to the total stress and the time dependence is allowed for to study the wave growth. The last term in (5.1) is the buoyancy term and $g' = g(\rho_\mathrm{w}-\rho_\mathrm{a})/\rho_\mathrm{w}$ is approximated as g, since $\rho_\mathrm{a}/\rho_\mathrm{w}\approx 1\times 10^{-3}$.

Integrating (5.1) over the volume bounded by the surface of the wave and vertical lines at successive wave crests extending from the wave surface to minus infinity,

$$\frac{\partial}{\partial t}\int\langle\langle\tfrac{1}{2}\Delta u_i^*\Delta u_i^*\rangle\rangle\,\mathrm{d}z+\langle\langle g\eta\,\Delta u_j^* n_j\rangle\rangle|_{z-\eta_-}=\langle\langle\Delta\sigma_{ij}^*\Delta u_i^* n_j\rangle\rangle|_{z-\eta_-}$$
$$-\int\left\langle\left\langle\Delta u_i^*\Delta u_j^*\frac{\partial U_i}{\partial x_j}\right\rangle\right\rangle\mathrm{d}z-\int\left\langle\left\langle\Delta\sigma_{ij}^*\frac{\partial \Delta u_i^*}{\partial x_j}\right\rangle\right\rangle\mathrm{d}z. \tag{5.2}$$

The outward normal is $\boldsymbol{n} = (-ak\mathrm{i}\,\mathrm{e}^{\mathrm{i}kz}, 1)[1+O(a^2k^2)]$, and $\langle\langle\,.\,\rangle\rangle$ denotes average over a wavelength (integral over a wavelength divided by the wavelength). A similar expression was derived by Davis (1972), who integrated upwards through the air flow; we find it more convenient to integrate downwards through the water.

Using the kinematic boundary condition, $\Delta w^*|_{z-\eta} = \mathrm{D}\eta/\mathrm{D}t$, the buoyancy term in (5.2) can be expressed to leading order in ak as

$$\langle\langle g\eta\,\Delta u_j^* n_j\rangle\rangle|_{z-\eta_-}=\left\langle\left\langle g\eta\frac{\mathrm{D}\eta}{\mathrm{D}t}\right\rangle\right\rangle(1+O(ak))=g\frac{1}{2}\frac{\partial}{\partial t}\langle\langle\eta^2\rangle\rangle(1+O(ak)), \tag{5.3}$$

which is the rate of change of the potential energy of the wave motion.

Returning to (5.2), the two terms on the left are, using (5.3), interpreted as the sum of the rate of change of the potential and kinetic energies, i.e. the rate of change of the

total wave energy, $\dot{E}$. The first term on the right of (5.2) is the rate of energy transfer across the interface. The second is the rate of working of the wave-induced velocity perturbations against the mean velocity gradient; this term is zero if the motion in the water is purely irrotational. The third is the rate at which wave energy is lost due to work done by the wave-induced stress perturbations, $\Delta\sigma_{ij}^*$; the contribution from the pressure is zero by incompressibility, but the viscous and turbulent stresses dissipate energy through this term.

In deep water, contributions to the third term arise from dissipation in the surface boundary layer in the water and the secondary straining of the irrotational motion in the bulk of the water flow. In the absence of breaking waves and if the turbulence in the surface boundary layer is weak, the latter dominates and is of $O(ER_w^{-1}T^{-1})$, where $R_w = L^2/(\nu T)$ is the Reynolds number of the wave motion, and T is the period of the wave motion (for a full discussion see e.g. Phillips 1977). In many experiments the surface boundary layer in the water is turbulent (Cheung & Street 1988) and a large energy dissipation may result. Furthermore, when the slope of the waves becomes larger the waves break and there is significant dissipation in the surface layer (Longuet-Higgins & Cokelet 1976; Phillips & Banner 1974).

In the present study we focus on the energy supplied to the wave motion from the wind above. This energy input arises through the first term on the right-hand side of (5.2) which is the rate at which the stresses do work at the surface of the wave; the subscript η_- denotes evaluation just below the surface, in the water. The stress and velocity are, however, continuous across the interface so that this term equals the rate of working of the stresses evaluated just above the wave, in the air flow (denoted $z = \eta_+$). Using these results, (5.2) becomes

$$\partial E/\partial t = \langle\langle \Delta\sigma_{ij}^* \Delta u_i^* n_j \rangle\rangle|_{z=\eta_+}, \tag{5.4}$$

which shows how the solutions obtained for the perturbations to the boundary layer above the wave may be used to calculate the energy flux into the wave motions. The distinction that (5.4) provides the flux into the wave motion is important: the air flow supplies additional energy into the water which drives surface currents (Hsu *et al.* 1982).

Previous studies have commonly calculated the growth rate of the wave by matching the pressure at the wave surface. The present method shows how the added energy transfer induced by the working of the Reynolds stresses should be calculated.

Substituting for the normal and expanding the stress tensor in (5.4), the energy flux into the wave motion correct to second order in ak is

$$\partial E/\partial t = \rho_a U_0^3 (ak)^2 \langle\langle [-p + \epsilon^2 \tau_{zz}]\, \bar{w} \sin(kx) + \epsilon^2 \tau \bar{u} \cos(kx) \rangle\rangle|_{z=\eta_+}, \tag{5.5}$$

where $\bar{u}$ and $\bar{w}$ are the amplitudes of the orbital velocity, associated with the wave motions, at the wave surface (see (2.14)).

In order to evaluate the energy flux, the perturbed stresses in (5.5), which are aligned with the Cartesian coordinates, must be related to the stress perturbations calculated in the preceeding sections, which are expressed in the displaced coordinates. To do this the coordinate transformation (2.8) is locally linearized and a matrix constructed which locally rotates from the displaced to the undisplaced coordinates. The details may be found in Belcher (1990). The pressure is isotropic so that it is unchanged by the rotation of axes. The Reynolds stresses, at the wave surface, in the two coordinate systems, are related by

$$\tau_{xx} = \tau_{XX} - 2\mathrm{i}\, \mathrm{e}^{\mathrm{i}X} T, \quad \tau_{zz} = \tau_{ZZ} + 2\mathrm{i}\, \mathrm{e}^{\mathrm{i}X} T, \quad \tau = \tau_d + \mathrm{i}\, \mathrm{e}^{\mathrm{i}X} (T_{XX} - T_{ZZ}). \tag{5.6}$$

T_{ij} is the unperturbed Reynolds stress tensor so that $T = T_{XZ} = 1$ in the dimensionless system used here. In analogy with the vertical velocity associated with the coordinate transformation, (2.9), the second terms on the right-hand sides of (5.6) are called the displacement stresses. The expression (5.5) shows that it is components of the shear stress that are in phase with the surface elevation that lead to an energy flux, hence the correction to the shear stress due to the displacement effect (which is in phase with the wave slope) does not contribute to the energy flux. Using these results, (5.5) becomes

$$\partial E/\partial t = \rho_a U_0^3 (ak)^2 \langle\langle (-p_d + \epsilon^2 \tau_{ZZ})\, \bar{w} \sin X + \epsilon^2 \tau_d\, \bar{u} \cos X - 2\epsilon^2 \bar{w} \sin^2 X \rangle\rangle|_{z=\eta_+}. \quad (5.7)$$

This shows that energy is transferred into the wave motion from three sources: components of (i) pressure and (ii) variance of the vertical turbulent velocity which are in phase with the wave slope; and (iii) the shear-stress perturbation which is in phase with the wave elevation (a mechanism discussed by Stewart 1967, and Longuet-Higgins 1969). The last term on the right-hand side of (5.7) is introduced when the normal stress, τ_{zz}, is transformed from the Cartesian to the displaced coordinates. This last term will be treated with the contribution to the energy flux from the shear stress (§5.3 below). Each of these three sources receives contributions from each of the three components of the solution for the air flow perturbations, namely (U), (S1), (S2).

5.1. *Contribution to the energy flux from the pressure perturbation*

The pressure perturbation induced by the non-separated sheltering effect of the undulation is listed as (A 7) in Appendix A; it is

$$\text{asym}\,(p_d^{(U)}) = -\frac{4\kappa^2\delta^2}{U^2(l)} \sin X = -\epsilon^2 \frac{4}{U^4(l)} \sin X, \quad (5.8a)$$

where asym ( ) denotes the asymmetric part of the perturbation that is in phase with the slope of the wave. This pressure perturbation has corrections caused by the IRS, ORS and FAD mechanisms which are smaller than (5.8*a*) by $O(\delta)$ (see the discussion of §1.1), which, formally, should be included since we calculate contributions to $\dot{E}$ from the (S1) and (S2) that are of the same order. The reliable results obtained using (5.8*a*) for the drag on a fixed undulation (BNH figure 8*b*) suggest that these corrections are numerically small and so in the present study they are neglected.

The perturbations to the air flow arising from the variations in surface properties also give rise to non-separated sheltering effects. The pressure perturbations in phase with the wave slope due to the varying surface velocity (S1) and the varying surface roughness length (S2) are given in (B 4) of Appendix B; they are

$$\text{asym}\,(p_d^{(S1)}) = \epsilon^2 \frac{2\bar{u}}{U^3(l)} \sin X, \qquad \text{asym}\,(p_d^{(S2)}) = -\epsilon^2 \frac{4\delta}{U^4(l)} \sin X. \quad (5.8b, c)$$

The (S1) contribution is of opposite sign to the (U) and (S2) components because, as discussed in §4.2.2, the phase of the orbital velocities leads to the boundary layer being thickened on the windward slope of the wave. Furthermore, since $\bar{u} = O(\delta)$, both the (S1) and (S2) effects lead to asymmetric pressure that are of $O(\delta)$ smaller than the effect of the undulation.

Using these results and the definition $\epsilon = u_*/U_0$, the energy flux due to the pressure asymmetry is

$$\frac{\partial E^{(\Delta p)}}{\partial t} = \rho_a u_*^2 U_0 (ak)^2 \bar{w} \frac{1}{2} \left[\frac{4}{U^4(l)} - \frac{2}{U^3(l)} \bar{u} + \frac{4\delta}{U^4(l)} \right]. \quad (5.9)$$

To proceed further the form of the motion in the water must be specified. For deep-water gravity waves, where $U_0 \bar{u} = c$,

$$\frac{\partial E^{(\Delta p)}}{\partial t} = \rho_a u_*^2 c(ak)^2 \frac{1}{2}\left[\frac{4}{U^4(l)} + \delta\left\{-\frac{\kappa c}{u_*}\frac{2}{U^2(l)} + \frac{4}{U^4(l)}\right\}\right]. \tag{5.10}$$

5.2. *Contribution to the energy flux from the normal Reynolds stress*

The energy budget (5.7) shows that the part of the vertical component of the variance of the turbulent velocity which is in phase with the wave slope also contributes to the energy flux and the discussion of §3.1 suggests that it can be calculated using the relation $\tau_{zz} = -\beta\tau_a$. The shear-stress perturbation induced by the undulation is in phase with the wave slope at $O(\delta)$, but the factor ϵ^2 then means that this contribution to the energy flux is $O(\delta)$ smaller than the non-separated sheltering pressure effect.

The solutions (A 3), (A 4) and (A 5) in Appendix A show that the leading-order normal-stress perturbation induced by the undulation that is in phase with the wave slope is

$$\text{asym}\,(\tau_{zz}^{(U)}) = \frac{2\pi\beta}{U^2(l)}\delta \sin X, \tag{5.11a}$$

and the relevant perturbations induced by the (S1) and (S2) effects are found from (B 2) and (B 3); they are

$$\text{asym}\,(\tau_{zz}^{(S1)}) = -\frac{2\pi\beta}{U(l)}\bar{u}\delta \sin X, \qquad \text{asym}\,(\tau_{zz}^{(S2)}) = \frac{4\pi\beta}{U^2(l)}\delta^2 \sin X. \tag{5.11b, c}$$

The energy flux due to the normal stress is then

$$\frac{\partial E^{(\Delta\tau_{zz})}}{\partial t} = \rho_a u_*^2 U_0(ak)^2 \bar{u}\tfrac{1}{2} 2\pi\beta\left[\frac{\delta}{U^2(l)} - \bar{u}\frac{\delta}{U(l)} + \frac{2\delta^2}{U^2(l)}\right], \tag{5.12}$$

so that for a deep-water gravity wave

$$\frac{\partial E^{(\Delta\tau_{zz})}}{\partial t} = \rho_a u_*^2 c(ak)^2 \tfrac{1}{2} 2\pi\beta\left[\frac{\delta}{U^2(l)} + O(\delta^2)\right]. \tag{5.13}$$

The $O(\delta^2)$ terms arise from the perturbations induced by the (S1) and (S2) variations and are negligible.

5.3. *Contribution to the energy flux from the shear stress*

Shear-stress perturbations in phase with the wave elevation contribute to the energy flux, but the displacement correction to the vertical component of the normal stress reduces this part of the energy flux. Furthermore, although the shear-stress perturbation is in phase with the wave height at zeroth order in δ, the energy flux due to the (U)-component of the shear-stress perturbation is of the same order as the contribution from the pressure because of the ϵ^2 factor in (5.7). The near cancellation of the leading-order contributions reduces the formal ordering of this part of the energy flux, see below. From (A 4), (A 5) and (B 3), the relevant components of the shear stress are

$$\text{sym}\,(\tau^{(U)}) = (2/U^2(l))[1 + \delta(4\gamma + 1 - \ln(z_m/z_0))]\cos X, \tag{5.14a}$$

$$\text{sym}\,(\tau^{(S1)}) = -\bar{u}(2/U(l))[1 + \delta(2\gamma - \ln(z_m/z_0))]\cos X, \tag{5.14b}$$

$$\text{sym}\,(\tau^{(S2)}) = (2\delta/U^2(l))[1 + \delta(2\gamma - \ln(z_m/z_0))]\cos X, \tag{5.14c}$$

where sym( ) denotes the symmetric part of the perturbation that is in phase with the wave elevation. The energy flux due to these perturbations is

$$\frac{\partial E^{(\Delta\tau)}}{\partial t} = \rho_a u_*^2 U_0 (ak)^2 \bar{w} \frac{1}{2}\left[2\left(\frac{1}{U^2(l)} - 1\right) + \frac{2}{U^2(l)}\delta(4\gamma + 1 - \ln(z_m/z_0)) \right.$$
$$\left. - \bar{u}\frac{2}{U(l)}\{1 + \delta(2\gamma - \ln(z_m/z_0))\} + \frac{4}{U^2(l)}\delta\{1 + \delta(2\gamma - \ln(z_m/z_0))\}\right]. \quad (5.15)$$

The first bracketed term on the right of (5.15) is due to the leading-order shear stress induced by the undulating surface, $2/U^2(l)$, minus the shear stress from the displacement part of the normal stress, -2. These two terms cancel in the limit of $\delta \to 0$ (when $U(l) \to 1$) and their difference is small whenever the present theory applies ($\delta \ll 1$):

$$1/U^2(l) - 1 \sim O(\delta \ln(1/\delta)),$$

from (3.1) and the definition $U_0 = (\epsilon/\kappa)\ln(h_m/z_m)$. Hence the contribution to the energy flux from $\Delta\tau^{(U)}$ and the displacement part of the normal stress nearly cancel, leading to a positive contribution to the energy flux that is of $O(\delta \ln(1/\delta))$ smaller than the NSS pressure perturbation.

For deep-water gravity waves, (5.15) becomes

$$\frac{\partial E^{(\Delta\tau)}}{\partial t} = \rho_a u_*^2 (ak)^2 \tfrac{1}{2} c\left[2\left(\frac{1}{U^2(l)} - 1\right) + \frac{2\delta}{U^2(l)}\left\{4\gamma + 3 - \frac{\kappa c}{u_*}(U^2(l) + 1)\right\} + O(\delta^2)\right]. \quad (5.16)$$

5.4. *Growth of the wave*

In order to calculate the growth rate of the wave, it is necessary to calculate the energy density of the waves and use the results (5.9), (5.12) and (5.15) for the energy flux into the wave motion to construct an equation for the evolution of the energy density.

The energy density of the wave motion is

$$E = \tfrac{1}{2}\rho_w a^2 c^2 k, \quad (5.17)$$

e.g. Phillips (1977). The amplitude of the wave is then governed by

$$\beta = 2\dot{a}/a = \dot{E}/E. \quad (5.18)$$

There is a variety of notation in the literature. Following Plant (1984), we use β to denote the (dimensional) growth rate of the spectral intensity of a wave of particular wavenumber, or, equivalently, the energy density of the wave. Miles (1957) uses β to denote the imaginary part of the non-dimensional pressure perturbation.

Using the expressions for the energy flux with (5.18),

$$\beta = \frac{\dot{E}}{E} = \frac{\rho_a}{\rho_w}\frac{u_*^2 k}{c} C_\beta = \frac{\rho_a}{\rho_w}\frac{u_*^2 k}{c}[C_\beta^{(U)} + C_\beta^{(S1)} + C_\beta^{(S2)}], \quad (5.19a)$$

where the growth rate coefficient, C_β, has been written by grouping the components from each of the three parts of the air flow solution, namely (U), (S1), and (S2), so that

$$C_\beta^{(U)} = \frac{4}{U^4(l)} + 2\left[\frac{1}{U^2(l)}\left(1 + \delta\left\{4\gamma + 1 - \frac{\kappa c}{u_*}\right\}\right) - 1\right] + \frac{2\delta\pi\beta}{U^2(l)} + O(\delta^2), \quad (5.19b)$$

$$C_\beta^{(S1)} = -2\delta\frac{\kappa c}{u_*}\left(\frac{1}{U^2(l)} + 1\right) + O(\delta^2), \quad (5.19c)$$

$$C_\beta^{(S2)} = 2\delta\left(\frac{2}{U^4(l)} - \frac{1}{U^2(l)}\right) + O(\delta^2). \quad (5.19d)$$

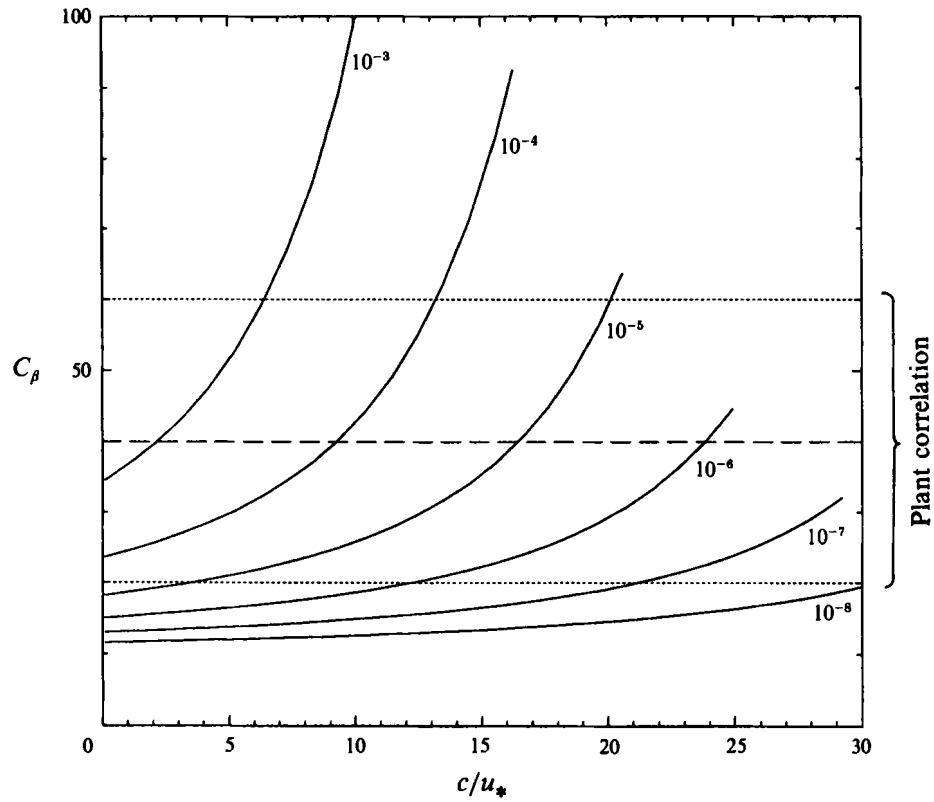

FIGURE 11. Variation of the amplitude growth rate coefficient with c/u_* for values of the relative roughness $kz_0 = 10^{-3}$, 10^{-4}, 10^{-5}, 10^{-6}, 10^{-7}, 10^{-8}. Curves truncated when $(c+u_*)/U_0 = \frac{3}{4}$.

In each case the first term is due to the pressure and the second the shear stress, and the third term in the undulation coefficient is due to the asymmetry in the normal Reynolds stress.

The right-hand side of (5.19*a*) is independent of a, so that the wave amplitude grows exponentially at a rate $\frac{1}{2}\beta$ and the wave energy, E, at a rate β. Furthermore, (5.19*a*) shows that the growth rate is strongly dependent on the friction velocity, u_*, which is determined by the Reynolds number of the flow when the wave surface is aerodynamically smooth, or by the height of the ripples when the wave surface is aerodynamically rough.

5.5. *Variation of the growth rate and comparison with other studies*

Our analysis shows that C_β is dependent on the three parameters, δ, c/u_* and $U(l)$. The parameter δ is related to ϵ, the basic small parameter of the problem, by $\delta = \epsilon/(\kappa U(l))$. Furthermore, as shown in §3.4, $\epsilon \sim (u_* + c)/U_B(L)$ (recall that $U_B(L)$ is the unperturbed velocity at a height $L = 2\pi/k$ in the frame where there is no mean motion in the water, i.e. the unsteady frame). For a logarithmic unperturbed velocity,

$$\epsilon \sim \frac{1 + c/u_*}{(1/\kappa)\ln(L/z_0)}, \tag{5.20}$$

so that ϵ, and hence δ, are fixed by the wave speed relative to the wind speed, c/u_*, and the ratio of the lengthscales L/z_0 (which is proportional to the Reynolds number of the flow, $Re_L = Lu_*/\nu$, for smooth interfaces). The values of both of these dimensionless

	(*a*) Laboratory				(*b*) Ocean			
	Δp	$\Delta\tau_{zz}$	$\Delta\tau$	Total	Δp	$\Delta\tau_{zz}$	$\Delta\tau$	Total
(U)	48	16	19	83	69	15	20	104
(S1)	−1	0	−1	−2	−11	0	−7	−18
(S2)	12	0	7	19	9	0	5	14
Total	59	16	25	100	67	15	18	100

TABLE 1. Percentage contributions to the growth rate: (*a*) laboratory experiments, $L/z_0 = 10^3$, $c/u_* = 1$ and $\delta = 0.26$; (*b*) typical oceanic values, $L/z_0 = 10^6$, $c/u_* = 10$ and $\delta = 0.12$

parameters commonly differ between laboratory and oceanic applications. The dimensionless wave speed, c/u_*, also leads to direct variations in C_β since $C_\beta^{(S1)}$ is linearly dependent on c/u_*.

Finally, all the contributions to C_β are dependent on

$$U(l) = \frac{U_B(l) - c}{U_B(h_m) - c}, \tag{5.21}$$

which is determined by the shape of the unperturbed velocity profile, and the ratio L/z_0 (which determines h_m and l), and is a measure of the shear across the middle layer. The leading-order contribution to C_β is proportional to $U^{-4}(l)$, so that this effect gives a substantial variation in wave growth rate with L/z_0. If the atmosphere is stratified, then the shear in the approach flow can be significantly different from that in a logarithmic profile and hence the growth rate can be altered (the effect of stratification on the drag force of a stationary undulation is currently being studied).

The effect of the variation of c/u_* and kz_0 on the growth rate coefficient C_β is plotted in figure 11. The curves have been truncated when $(u_* + c)/U_B(L) = \frac{1}{2}$. The figure shows that varying the parameters can change the growth rate coefficient by two orders of magnitude. Also shown on figure 11 are the values obtained empirically by Plant (1984), which are discussed below.

Table 1 shows the percentage contributions to the growth rate from each of the three physical mechanisms and from each of the three components of the air flow solution. In table 1 (*a*) the parameters are chosen to be representative of the values in laboratory experiments, and in table 1 (*b*), typical oceanic values have been selected. The table shows that, for both laboratory and oceanic applications, although the dominant contribution to the energy flux comes from the asymmetric pressure perturbation induced by the undulating wave shape, the overall result is strongly affected by the inclusion of the effects of the shear and normal stress variations induced by the undulation, and the effects of the varying surface properties. Hence the growth rate may be significantly larger than estimated by previous theories and correlations that are based on only the asymmetric pressure effect (e.g. Plant 1984). Kendall (1970) suggested that the shear stress only transmits about 3% of the energy flux, but table 1 (*a*) (which uses parameter values close to those of Kendall 1970) shows that shear stress contributes to 25% of the energy flux. Hence, although the contribution to the energy flux from the shear stress is formally of $O(\delta \ln(1/\delta))$ smaller than the sheltering effect, it can significantly contribute to the growth rate.

Throughout the present study the discussion has focused on cocurrent wind-wave flow, but the analysis is also valid when the wind blows against the direction of wave propagation. In such a countercurrent wind-wave flow, the wave phase speed is negative and (5.19*a*) shows that the waves are quenched exponentially. When the wind-

wave flow is cocurrent, the (S1) perturbations, induced by the orbital motions in the wave, extract energy from the wave motions, but these effects lead to an energy flux proportional to c^2, (5.19c), so that in countercurrent flow, when $c \to -c$, they continue to quench the waves. Hence all the effects tend to reduce the wave motions, so the wave amplitude in countercurrent flow decreases faster than it increases in cocurrent flow.

The wave growth rate, (5.19), may be rewritten in terms of the period of the wave motion, T, so that

$$\beta = \frac{\rho_a}{\rho_w} \frac{2\pi}{T} \frac{u_*^2}{c^2} C_\beta. \tag{5.22}$$

This has the form postulated by Plant (1984), which he derived by correlating laboratory and field experiments and not from any solutions to the equations. In order to fit the experimental data, Plant (1984) suggested that C_β is constant and equal to 40 ± 20. In the limit that $\epsilon \to 0$, the theoretical value of C_β has a finite and non-zero contribution from only the NSS pressure effect; namely $C_\beta \to 4$ (since $\delta \to 0$ and $U(l) \to 1$ as $\epsilon \to 0$) and is independent of c/u_*. For finite values of ϵ, however, C_β is significantly larger and increases with c/u_* (see figure 11). For example, when $kz_0 = 10^{-4}$, a value that is intermediate between those typical in the laboratory experiments and the oceanic values, $\ln^{-1}(1/kz_0) = 0.11$ and C_β ranges from about 23 (when $c/u_* = 0$) upwards to about 40 when $c/u_* = 10$. These values are then consistent with Plant's suggestion. The reason that the asymptotic value of 4 (as $\epsilon \to 0$) is so different from the value at physically reasonable parameter values is that the asymptote depends on $\ln(1/kz_0)$ tending to infinity, which happens extremely slowly.

Figures 12(a) and 12(b) show comparisons of the theoretical prediction of the growth rate of the energy density, β, normalized on the frequency of the wave, $f = 1/T$, together with the laboratory data collated by Plant (1984). In figure 12(a), L/z_0 has the value 10^3, which is representative of the laboratory experiments, and in figure 12(b), L/z_0 is 10^5, representative of ocean waves. The prediction (5.10) agrees well with the experimental data through a wide variety of conditions, so the requirement that $(c+u_*)/U_B(L)$ be small is not severe.

The asymptotic theory of van Duin & Janssen (1992), which includes the analysis of Jacobs (1987) as a special case, uses an eddy viscosity for the shear stress throughout the flow. We have argued (§3.1) that this is inappropriate and leads to a growth rate that is a factor of $O(1/\epsilon)$ too large. Denoting their growth rate as β_{VDJ} and rewriting in our notation, van Duin & Janssen (1992) find that

$$\beta_{VDJ} = \frac{\rho_a}{\rho_w} \frac{2\pi}{T} 2 \frac{u_*^2}{c^2} (1 + \tfrac{1}{4}n) \left(\frac{\kappa}{\bar{\epsilon}} - \frac{\kappa c}{u_*} \right), \tag{5.23}$$

i.e. $C_{VDJ} = 2(1+\frac{1}{4}n)(\kappa/\bar{\epsilon} - \kappa c/u_*)$, which is indeed $O(1/\epsilon)$ larger than our value. In (5.23), $n = O(1)$ and determines the precise form of the eddy-viscosity model (Jacobs' mixing-length result emerges when $n = 0$). Furthermore, $\bar{\epsilon} = u_*/U_B(L)$, whereas we have $\epsilon = u_*/(U_B(L) - c)$ – the magnitudes are the same for small wave speeds. Although C_{VDJ} is formally $O(1/\epsilon)$ larger than our value, in practice our formula gives values that are of the same magnitude or larger. For example, substituting $kz_0 = 10^{-4}$ and $c = 0$ gives $C_{VDJ} \approx 18(1+\frac{1}{4}n)$, which is similar to the value of 23 from our model. Furthermore, when $c/u_* = 10$, $C_{VDJ} = 10(1+\frac{1}{4}n)$, which is four times smaller than the value of 40 obtained with our model. So, somewhat surprisingly, although C_{VDJ} is formally larger, for practical values of the parameters, it may give smaller growth rates than the present result (5.22).

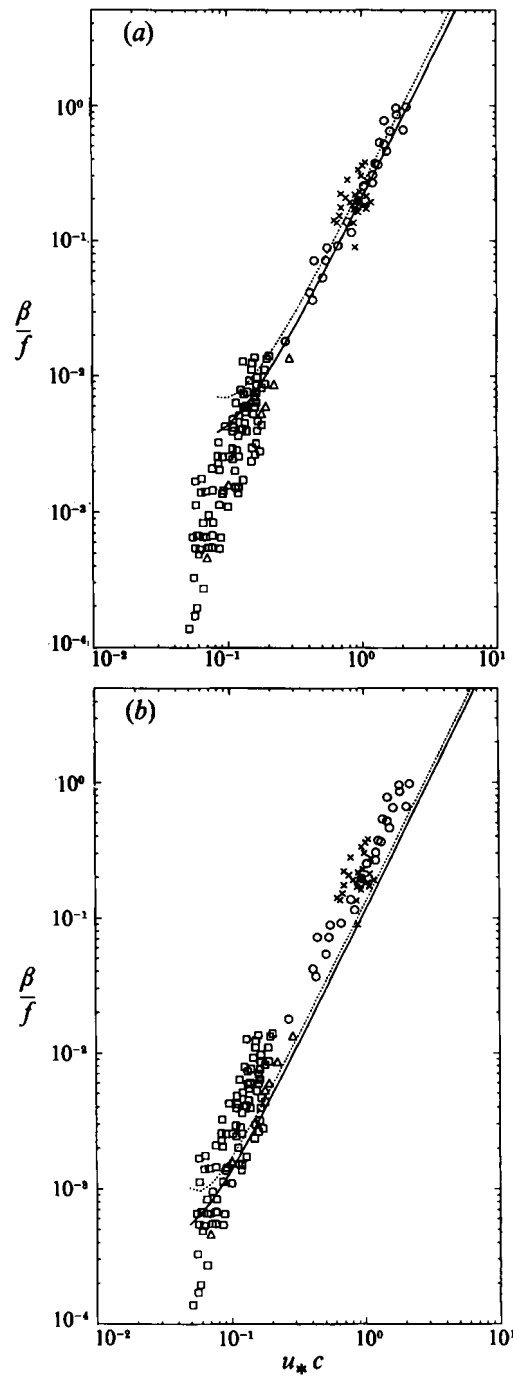

FIGURE 12. The growth rate of the energy density of the wave (twice the amplitude growth rate) due to the effect of the asymmetric pressure, made non-dimensional on the wave frequency f. The theoretical curves are compared with the data collated by Plant (1984). The upper group of experimental points is mainly from wave tank experiments and the lower group from oceanic experiments. (*a*) $L/z_0 = 10^3$ typical of the wave tank experiments, (*b*) $L/z_0 = 10^5$ typical of the ocean experiments.

Al-Zanaidi & Hui (1984) have used the results of their numerical model, which uses a two-equation closure model for the turbulence, to construct an empirical relation for the growth rate; it is

$$\beta_{\mathrm{AZH}} = \frac{\rho_a}{\rho_w}\frac{2\pi}{T}\frac{0.06}{\bar{\epsilon}^2}\left(\frac{u_*}{c}-\bar{\epsilon}\right)^2, \tag{5.24}$$

which has a different scaling again. With the parameters used above, this formula yields a value $C_{\mathrm{AZH}} \approx 32$ for all wave speeds, which is between our value at $c/u_* = 0$ (where $C_\beta = 23$) and $c/u_* = 10$ (where $C_\beta = 40$), despite the difference in the formal scaling.

The expression (5.22) for the wave growth rate shows that the original assumption that the flow perturbations are quasi-steady is valid up till a time

$$O\left(\frac{\rho_w}{\rho_a}T\frac{c^2}{u_*^2}\right), \tag{5.25}$$

which is certainly large for an air–water system, so the steady flow solutions found here are of practical value.

6. Perturbation drag force on the wave

The presence of the wave increases the wavelength-averaged drag force on the surface. BNH calculate the drag over rigid topography and here the results are generalized for a moving surface.

The force on the wave surface is computed by integrating the normal component of the stress tensor, σ_{ij}, along the surface,

$$F_i = \int \sigma_{ij} n_j \,\mathrm{d}S, \tag{6.1}$$

where $\boldsymbol{n}$ is the normal into the water. Taking the horizontal component and substituting for the stress tensor, the perturbation drag force becomes

$$\Delta F = -\rho_a U_0^2 ak \int_{Z-kz_0} \epsilon^2 \tau_d \,\mathrm{e}^{\mathrm{i}kx}\,\mathrm{d}X - \rho_a U_0^2 (ak)^2 \int_{Z-kz_0} (p_d - \epsilon^2 \tau_{XX})\,\mathrm{i}\,\mathrm{e}^{\mathrm{i}kx}\,\mathrm{d}X \tag{6.2}$$

correct to second order in ak, and the integrals are taken over one wavelength. The linear part of the stress perturbation immediately integrates to zero by periodicity in the x-direction, and so the dominant contribution to the drag force is $O((ak)^2)$ and is due to the component of the normal stress (both the dynamic pressure and the normal Reynolds stress) in phase with the wave slope together with the $O((ak)^2)$ stress perturbation. We focus on the pressure force – the second integral in (6.2).

The pressure perturbation from the undulation component of the solution is in phase with the slope at $O(\delta^2)$, and the Reynolds stress at $O(\delta)$; however, the factors of ϵ^2 in (6.2) then mean that the pressure term is the largest in the second integral. Similar scaling arguments show that the dominant contributions to the drag force from the (S1) and (S2) components of the solution are also due to the asymmetric pressure perturbations, but because the amplitude of the orbital velocity and roughness changes are $O(\delta)$ smaller, their contributions to the drag are $O(\delta)$ smaller than from the (U) part of the solution.

The pressure perturbations required to calculate the change in the drag force are the same as used in the calculation of the wave growth rate and are discussed in §5.1.

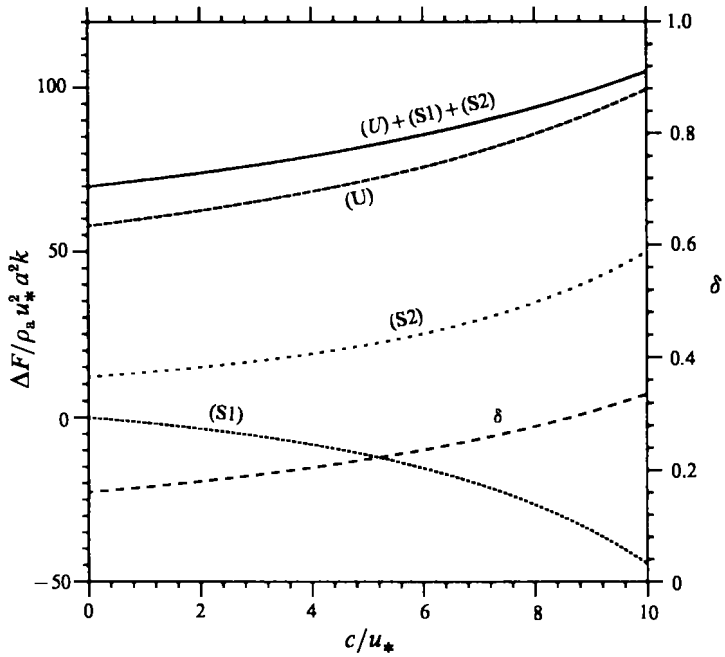

FIGURE 13. Variation of the normalized drag on the wave surface, $\Delta F/(\rho_a u_*^2 a^2 k)$, with wave speed, c/u_*, for $kz_0 = 10^{-4}$. The variation of δ is also shown (refer to scale on right).

Overall, for the flow over deep-water gravity waves, the leading-order perturbation drag force from the asymmetric pressure is

$$\Delta F = \rho_a u_*^2 a^2 k \frac{4\pi}{U^4(l)}\left[1 + \frac{\delta}{U(l)} - \delta U^2(l)\frac{1}{2}\frac{\kappa c}{u_*}\right]. \tag{6.3}$$

When the present theory is valid, the contribution from the undulation part of the solution dominates, and the overall drag is increased.

Figure 13 shows the variation of the normalized pressure force on the wave surface, $\Delta F/(\rho_a u_*^2 a^2 k)$, with the dimensionless wave speed, c/u_*, for the various contributions from (U), (S1), and (S2) as well as the total. Notice in particular the large numerical value of this drag coefficient. The variation of the drag with slope is quadratic and has been displayed by BNH (their figure 11) for the fixed undulation ($c/u_* = 0$).

7. Discussion

We have found asymptotic solutions for the linear perturbations (for small wave slope ak) to a turbulent boundary layer passing over a moving gravity wave in the limit $(u_* + c)/U_B(L) \to 0$. With this condition the analysis can be based on an extension of the four-layer theory developed by HLR for the flow over a low hill. Within the linear framework, the effects of the undulating boundary and the varying surface conditions can be analysed independently. The solution has been constructed by combining (with some modification) the theory of HLR, BNH and Belcher *et al.* (1990) for the perturbations due to a rigid undulation and due to a varying roughness length. A particular feature of these asymptotic theories is that at leading order the turbulent stresses can be calculated by the mixing-length model provided that it is truncated at the top of the inner region. If this is not done and the mixing-length model is used

throughout the flow, the magnitude of the growth rate is a factor $O(1/\epsilon)$ too large (van Duin & Janssen 1992; Jacobs 1987).

To make use of this asymptotic theory it is necessary to review the conditions for the solutions to be valid. Firstly, the condition for linearization of the perturbations is $ak \ll 1$. For the flow over rigid undulating surfaces, the linear theory has been found to give useful results (Mason & King 1985; BNH) for slopes up to about $\frac{1}{3}$, when separation occurs. The results for the flow over a gravity wave are expected to be about as good up to the same limit. Secondly, we have found approximate asymptotic solutions for the linear perturbations. The asymptotic analysis is valid if $\delta \ll 1$. In practice δ can often be as large as $\frac{1}{3}$ or $\frac{1}{4}$, and the theory provides useful results if δ is as large as $\frac{1}{2}$. An equivalent condition to the requirement of small δ is that $|u_* + c|/U_B(L) \ll 1$.

Using the expression (5.22) for the growth rate of the wave, we may give order of magnitude estimates for the mechanisms which have been proposed to account for the wave growth that are listed in the introduction.

M. The Miles mechanism

Miles (1967) recognized that the turbulent stresses may profoundly affect the wave growth and we have shown that when $|u_* + c|/U_B(L) \ll 1$, the matched height lies within the ISL, where the leading-order perturbations are determined by the perturbation shear stress. Hence, it is inappropriate to apply the inviscid Miles (1957) theory. It is, however, instructive to compare with the other mechanisms the magnitude of the growth rate predicted by his theory. According to the Miles theory, the energy transfer rate is

$$E = \rho_a c L[-(U''/U')\langle\langle w^2\rangle\rangle]_{z-kz_m}.$$

Using our expression for the vertical velocity perturbation, we find that the growth rate, β, is given by

$$\beta = \frac{\rho_a}{\rho_w}\frac{2\pi}{T}\frac{u_*^2}{c^2}\frac{\pi^2}{4}\frac{1}{U^2(l)}\frac{1}{\delta}e^{-1/\delta} = O\left(\frac{\rho_a}{\rho_w}\frac{2\pi}{T}\frac{u_*^2}{c^2}\frac{1}{\delta}e^{-1/\delta}\right),$$

which is smaller than the contribution from the asymmetric pressure (see below) by $O(1/\delta e^{-1/\delta})$.

NSS. Non-separated sheltering

The undulation induces an asymmetric pressure perturbation at the surface of the wave, caused by the action of the Reynolds shear stress within the inner region. This effect leads to the dominant contribution to the flux of energy to the wave, and the resulting growth rate is

$$O\left(\frac{\rho_a}{\rho_w}\frac{2\pi}{T}\frac{u_*^2}{c^2}\right).$$

IRS. Inner-region Reynolds stress effects

Within the inner region, the perturbations to the shear stress which are in phase with the topography, and the changes to the normal Reynolds stress which are in phase with the wave slope lead to contributions to the growth rate. The shear stress leads to a growth rate contribution of

$$O\left(\frac{\rho_a}{\rho_w}\frac{2\pi}{T}\frac{u_*^2}{c^2}\delta\ln(1/\delta)\right),$$

which is smaller than the sheltering effect by $O(\delta\ln(1/\delta))$.

The normal stresses lead to a smaller contribution to the growth rate of

$$O\left(\frac{\rho_a}{\rho_w}\frac{2\pi}{T}\frac{u_*^2}{c^2}\delta\right).$$

ORS. Outer-region Reynolds stress effects

The changes to the Reynolds stresses in the outer region may affect the surface pressure through the elliptic effects in the equations, see BNH. These effects lead to a surface pressure asymmetry of $O(\rho_a U_0^2(H/L)\epsilon^2\delta^2)$ (see BNH), leading to a growth rate of

$$O\left(\frac{\rho_a}{\rho_w}\frac{2\pi}{T}\frac{u_*^2}{c^2}\delta^2\right).$$

The curvature of the mean streamlines leads to changes in the surface pressure through this same dynamical process and leads to a contribution to the growth rate of the same order of magnitude.

S1. Orbital velocity effects

The orbital velocity associated with the motion of the water induces perturbations to the air flow, which lead to an asymmetric pressure which is exactly out of phase with the wave slope, and so inhibits wave growth. The growth rate from this mechanism has magnitude

$$O\left(-\frac{\rho_a}{\rho_w}\frac{2\pi}{T}\frac{u_*}{c}\delta\right),$$

which grows only linearly with u_*/c.

S2. Variable roughness effects

We have included, as a heuristic calculation, a variation in the roughness length of the wave surface induced by the variation in the surface shear stress along the surface of the wave. This gives rise to perturbations which increase the asymmetry of the perturbed boundary layer, and so lead to an asymmetric surface pressure which then induces a growth of the wave amplitude. The magnitude of the contribution to the growth rate from this mechanism is

$$O\left(\frac{\rho_a}{\rho_w}\frac{2\pi}{T}\frac{u_*^2}{c^2}\delta\right).$$

Gent & Taylor (1976) found that the inclusion of varying surface roughness significantly increased the energy flux to the wave, but they did not scale the amplitude of the roughness length variation on the slope of the wave, hence they obtain a contribution to the growth rate of

$$O\left(\frac{\rho_a}{\rho_w}\frac{2\pi}{T}\frac{u_*^2}{c^2}\delta\frac{\ln(z_1/z_2)}{ak}\right),$$

i.e. a larger relative contribution for smaller slope (they kept the amplitude of the roughness variation constant for all slopes). We find a smaller but nevertheless significant contribution to the wave growth.

This summary of the magnitudes of the processes controlling the wave growth show

that the leading-order contribution arises from the asymmetric displacement of the outer-region flow caused by the $O(\delta^2)$ thickening of the inner region in the lee of the wave. This we term non-separated sheltering. The theoretical value of the shear-stress perturbation at the crest of the wave at both the wave surface and top of the inner region is in good agreement with values measured in the laboratory (§4.3) and therefore, by an argument developed in BNH, the pressure asymmetry due to non-separated sheltering is reliably calculated by the theory. The detailed discussion of §5.4 shows, however, that the $O(\delta \ln(1/\delta))$ contribution from the shear stress and the $O(\delta)$ corrections, which arise from the IRS, S1 and S2 effects, collectively contribute significantly to the wave growth. Hence methods that determine the wave growth from the pressure effect only may significantly underestimate the growth rate.

Despite the restriction that $|u_* + c|/U_B(L) \ll 1$, the theory has been shown to describe a large portion of the experimental observations of the wave growth rate made at sea and in the laboratory.

During the course of this research we benefited from useful conversations with Alan Townsend, for which we are grateful. Thanks are also due to Lady Jeffreys, who kindly sent some original offprints of Sir Harold's original papers. S.E.B. is grateful for the financial support of the SERC under a CASE award with AERE Harwell. We are also grateful for the many useful comments made by the referees.

Appendix A. Solutions for the flow over an undulation

The unperturbed mean velocity profile is given by

$$\bar{U}_B(z) = (u_*/\kappa)\ln(z/z_m),$$

where the matched height is given by

$$z_m = z_0 e^{\kappa c/u_*}.$$

The solutions are expressed in terms of the displaced coordinates, which are related to the Cartesian coordinates by

$$kx = X - ak\,i e^{iX-Z}, \quad kz = Z + ak\,e^{iX-Z}. \tag{A 1}$$

Mean flow quantities are made non-dimensional using $U_0 = U_B(h_m)$ and the Reynolds stress components on ρu_*^2. The linear perturbations in the Cartesian coordinates are related to those in the displaced coordinates by

$$\left.\begin{gathered} u(z) = u_d(Z), \quad w(z) = i e^{iX-Z} + w_d(Z), \quad p(z) = p_d(Z), \\ \tau_{xx}(z) = \tau_{XX} - 2i e^{iX-Z}, \quad \tau_{zz}(z) = \tau_{ZZ} + 2i e^{iX-Z}, \quad \tau(z) = \tau_d + i e^{iX-Z}(T_{XX} - T_{ZZ}). \end{gathered}\right\} \tag{A 2}$$

The following expressions are the solutions for the perturbations in the displaced coordinates.

A.1. *Inner-surface layer*

The vertical coordinate scales on z_m and is $\eta = Z/(kz_m) \sim (1/\delta)e^{1/\delta}Z$.

$$u_d \sim -(1/U(l))[(\delta\hat{\tau}^{(0)}(\eta_0) + \delta^2\hat{\tau}^{(1)}(\eta_0) + O(\delta^3))\ln(\eta/\eta_0) + O(kz_m)]e^{iX}, \tag{A 3a}$$

$$w_d \sim -(1/U(l))[O(kz_m)]e^{iX}, \tag{A 3b}$$

$$\tau_d \sim -(2/U^2(l))[\hat{\tau}^{(0)}(\eta_0) + \delta\hat{\tau}^{(1)}(\eta_0) + O(\delta^3, kz_m)]e^{iX}, \tag{A 3c}$$

$$p_d \sim [\hat{\sigma}^{(0)} + O(\delta^2, kz_m)]e^{iX}. \tag{A 3d}$$

With $\eta_0 = z_0/z_m$ and

$$\hat{\tau}^{(0)} = \hat{\sigma}^{(0)}, \quad \hat{\tau}^{(1)} = (1 + i\pi + 4\gamma - \ln(z_m/z_0))\,\hat{\sigma}^{(0)}, \tag{A 4}$$

$$\hat{\sigma}^{(0)} = -1. \tag{A 5}$$

A.2. *Shear-stress layer*

The order-one vertical coordinate in the shear-stress layer is $\zeta = Z/kl \sim Z/\delta$.

$$u_d \sim -(\hat{\sigma}^{(0)}/U(l))[1 + \delta[1 - \ln\zeta + A_1 K_0(2(i\zeta)^{\frac{1}{2}})] + O(\delta^2)]\,e^{iX}, \tag{A 6a}$$

$$w_d \sim -(\hat{\sigma}^{(0)}/U(l))[-2i\delta\kappa^2\zeta + O(\delta^2)]\,e^{iX}, \tag{A 6b}$$

$$\tau_d \sim -(2\hat{\sigma}^{(0)}/U^2(l))[-1 + A_1\zeta\,\partial K_0/\partial\zeta + O(\delta)]\,e^{iX}, \tag{A 6c}$$

$$p_d \sim [\hat{\sigma}^{(0)} + \delta^2\hat{\sigma}^{(2)} + O(\delta^3)]\,e^{iX}, \tag{A 6d}$$

where

$$A_1 = -4, \quad \mathrm{Im}[\hat{\sigma}^{(2)}] = -4i\kappa^2\hat{\sigma}^{(0)}/U^2(l), \tag{A 7}$$

and Im denotes 'imaginary part of'.

A.3. *Middle layer*

The vertical coordinate is scaled on h_m so that $\hat{z} = Z/kh_m$. Furthermore, for a logarithmic approach flow, $\hat{z} \sim \epsilon^{\frac{1}{2}}Z$ and $kh_m = (\epsilon/\kappa)^{\frac{1}{2}}$.

$$u_d \sim -\left[\frac{1}{kh_m}\tilde{f}U' + \frac{\hat{\sigma}^{(0)}}{U}\left[1 + UU'\int^{\hat{z}}\frac{dz'}{U^2(h_m z')}\right] + O(kh_m)\right]e^{iX}, \tag{A 8a}$$

$$w_d \sim is\left[\tilde{f}U + kh_m\hat{\sigma}^{(0)}UU(z)\int^{\hat{z}}\frac{dz'}{U^2(h_m z')} + O(k^2h_m^2)\right]e^{iX}, \tag{A 8b}$$

$$p_d \sim [\hat{\sigma}^{(0)} + O(kh_m)]\,e^{iX}. \tag{A 8c}$$

A.4. *Upper layer*

The vertical coordinate is of order one. The vertical-velocity perturbations in the upper layer are, by construction, accounted for by the displaced coordinate system. Hence

$$u_d \sim [e^{iX-Z} + O(kh_m)], \quad w_d \sim [O(kh_m)], \quad p_d \sim -u_d. \tag{A 9}$$

Appendix B. Solutions for the flow over varying surface velocity

In this Appendix we state the solutions for the Fourier transforms of the perturbations to a turbulent boundary layer over a varying tangential surface velocity. The unperturbed velocity profile and non-dimensionalization scheme are the same as Appendix A.

The surface boundary conditions are

$$u = u(z_0), \quad w = 0 \quad \text{on} \quad z = z_0. \tag{B 1}$$

B.1. *Inner-surface layer*

In the ISL the vertical coordinate scales on z_m so that $\eta = Z/kz_m$.

$$u \sim u(z_0)[1 + (\delta\hat{\tau}^{(0)}(\eta_0) + \delta^2\hat{\tau}^{(1)}(\eta_0) + \delta^3\hat{\tau}^{(2)}(\eta_0))\ln(\eta/\eta_0) + O(\delta^3)]\,e^{iX}, \tag{B 2a}$$

$$w \sim u(z_0)[O(\delta\,e^{-1/\delta})]\,e^{iX}, \tag{B 2b}$$

$$\tau \sim u(z_0)(2/U(l))[\hat{\tau}^{(0)}(\eta_0) + \delta\hat{\tau}^{(1)}(z_0) + \delta^2\hat{\tau}^{(2)}(\eta_0) + O(\delta^3)]\,e^{iX}, \tag{B 2c}$$

$$p \sim -u(z_0)\,U(l)[\delta^2\hat{\sigma}^{(2)} + O(\delta^3)]\,e^{iX}. \tag{B 2d}$$

With $$\hat{\tau}^{(0)} = -1, \quad \hat{\tau}^{(1)} = \ln(z_m/z_0) - \tfrac{1}{2}(\mathrm{i}\pi + 4\gamma), \tag{B 3}$$

$$\hat{\sigma}^{(2)} = 2\mathrm{i}\kappa^2/U^2(l). \tag{B 4}$$

B.2. *Shear-stress layer*

As usual in the SSL, $\zeta = Z/kl$.

$$u \sim u(z_0)[\delta 2K_0(2\sqrt{(\mathrm{i}\zeta)}^{\frac{1}{2}}) + \delta^2[\hat{\sigma}^{(2)} + 2(\ln\zeta - 2)\,\zeta\,\partial K_0/\partial\zeta - K_0\ln\zeta + A_2 K_0 - \mathscr{F}(1/\zeta)] + O(\delta^3)]\,\mathrm{e}^{\mathrm{i}X}, \tag{B 5a}$$

$$w \sim u(z_0)[-\delta^2 2\kappa^2[1 + 2\zeta\,\partial K_0/\partial\zeta] + O(\delta^3)]\,\mathrm{e}^{\mathrm{i}X}, \tag{B 5b}$$

$$\tau \sim u(z_0)(2/U(l))[2\zeta\,\partial K_0/\partial\zeta + \delta[(2 - \ln\zeta + A_2)\,\zeta\,\partial K_0/\partial\zeta + (2\mathrm{i}\zeta(\ln\zeta - 2) - 1)\,K_0 - \mathscr{F}'] + O(\delta^3)]\,\mathrm{e}^{\mathrm{i}X}, \tag{B 5c}$$

$$p \sim -u(z_0)\,U(l)[\delta^2\hat{\sigma}^{(2)} + O(\delta^3)]\,\mathrm{e}^{\mathrm{i}X}, \tag{B 5d}$$

where $$A_2 = -2[3 + \ln(z_m/z_0) - \tfrac{3}{4}(\mathrm{i}\pi + 4\gamma)]. \tag{B 6}$$

$\mathscr{F}(1/\zeta)$ is the particular integral of

$$(\partial/\partial\zeta)(\zeta\,\partial\hat{u}_d/\partial\zeta) - \mathrm{i}\hat{u}_d = 1/\zeta,$$

which cannot be solved exactly, but there are the approximate results

$$\left.\begin{aligned} \mathscr{F} &\sim \tfrac{1}{2}\ln^2\zeta + 2\ln\zeta + 1 + O(\zeta\ln^2\zeta) \quad \text{as} \quad \zeta \to 0 \\ \mathscr{F} &\sim -1/\mathrm{i}\zeta + O(1/\zeta^2) \quad \text{as} \quad \zeta \to \infty. \end{aligned}\right\} \tag{B 7}$$

B.3. *Middle layer*

In the middle layer we scale $\hat{z} = Z/kh_m$, and U means $U(h_m\hat{z})$

$$u \sim u(z_0)\,\delta^2\frac{1}{kh_m}\left[\frac{2\kappa^2}{\mathrm{i}U(l)}U' + kh_m\hat{\sigma}^{(2)}\frac{U(l)}{U}\left[1 + UU'\int^{\hat{z}}\frac{\mathrm{d}z'}{U^2(h_m z')}\right] + O(k^2h_m^2)\right]\mathrm{e}^{\mathrm{i}X}, \tag{B 8a}$$

$$w \sim u(z_0)\,\delta^2\left[-\frac{2\kappa^2}{U(l)}U - kh_m\,\mathrm{i}\hat{\sigma}^{(2)}U(l)\,U\int^{\hat{z}}\frac{\mathrm{d}z'}{U^2(h_m z')} + O(k^2h_m^2)\right]\mathrm{e}^{\mathrm{i}X}, \tag{B 8b}$$

$$p \sim -u(z_0)\,\delta^2[\hat{\sigma}^{(2)}U(l) + O(kh_m)]\,\mathrm{e}^{\mathrm{i}X}. \tag{B 8c}$$

B.4. *Upper layer*

The vertical coordinate Z is of order one. Then

$$u \sim u(z_0)\,\delta^2\left[\frac{2\mathrm{i}\kappa^2}{U(l)}\mathrm{e}^{-Z} + O(kh_m)\right]\mathrm{e}^{\mathrm{i}X}, \quad w \sim w(z_0)\,\delta^2\left[-\frac{2\kappa^2}{U(l)}\mathrm{e}^{-Z} + O(kh_m)\right]\mathrm{e}^{\mathrm{i}X}, \quad p \sim -u. \tag{B 9}$$

REFERENCES

Abramowitz, M. & Stegun, I. R. 1972 *A Handbook of Mathematical Functions*. Dover.

Al-Zanaidi, M. A. & Hui, W. H. 1984 Turbulent air flow over water waves – a numerical study. *J. Fluid Mech.* **148**, 225–246.

Belcher, S. E. 1990 Turbulent boundary layer flow over undulating surfaces. PhD thesis, University of Cambridge.

Belcher, S. E., Newley, T. M. J. & Hunt, J. C. R. 1993 The drag on an undulating surface due to the flow of a turbulent layer. *J. Fluid Mech.* **249**, 557–596 (referred to herein as BNH).

Belcher, S. E., Xu, D. P. & Hunt, J. C. R. 1990 The response of a turbulent boundary layer to arbitrarily distributed two-dimensional roughness changes. *Q. J. R. Met. Soc.* **116**, 611–635.

Benjamin, T. B. 1959 Shearing flow over a wavy boundary. *J. Fluid Mech.* **6**, 161–205.

BRITTER, R. E., HUNT, J. C. R. & RICHARDS, K. J. 1981 Air flow over a 2-d hill: studies of velocity speed-up, roughness effects and turbulence. *Q. J. R. Met. Soc.* **107**, 91–110.

CHARNOCK, H. 1955 Wind stress on a water surface. *Q. J. R. Met. Soc.* **81**, 639.

CHEUNG, T. K. & STREET, R. L. 1988 The turbulent layer in the water at an air–water interface. *J. Fluid Mech.* **194**, 133–151.

DAVIS, R. E. 1972 Perturbed turbulent flow, eddy viscosity and the generation of turbulent stresses. *J. Fluid Mech.* **63**, 673–693.

DUIN, C. A. VAN & JANSSEN, P. A. E. M. 1992 An analytical model of the generation of surface gravity waves by turbulent air flow. *J. Fluid Mech.* **236**, 197–215.

GENT, P. R. & TAYLOR, P. A. 1976 A numerical model of air-flow above water waves. *J. Fluid Mech.* **77**, 105–128.

HARRIS, J. A. 1992 On the growth of water waves and the motions beneath them. PhD thesis, Stanford University.

HUNT, J. C. R. 1973 A theory of turbulent flow round two-dimensional bluff bodies. *J. Fluid Mech.* **61**, 625–706.

HUNT, J. C. R., LEIBOVICH, S. & RICHARDS, K. J. 1988 Turbulent shear flows over low hills. *Q. J. R. Met. Soc.* **114**, 1435–1471 (referred to herein as HLR).

HSU, C.-T., HSU, E.-Y. & STREET, R. L. 1981 On the structure of turbulent flow over a progressive water wave: theory and experiment in a transformed, wave-following coordinate system. *J. Fluid Mech.* **105**, 87–117.

HSU, C.-T., WU, H.-Y., HSU, E.-Y. & STREET, R. L. 1982 Momentum and energy transfer in wind generation of waves. *J. Phys. Oceanogr.* **12**, 929–951.

JACOBS, S. J. 1987 An asymptotic theory for the turbulent flow over a progressive wave. *J. Fluid Mech.* **174**, 69–80.

JANSSEN, P. A. E. M. 1982 Quasilinear approximation for the spectrum of wind generated ocean waves. *J. Fluid Mech.* **48**, 91–127.

JEFFREYS, H. 1925 On the formation of water waves by wind. *Proc. R. Soc. Lond.* A **107**, 189–206.

KENDALL, J. M. 1970 The turbulent boundary layer over a wall with progressive surface waves. *J. Fluid Mech.* **41**, 259–281.

KINSMAN, B. 1984 *Wind Waves: Their Generation and Propagation on the Ocean Surface.* Dover.

LIGHTHILL, M. J. 1962 Physical interpretation of the theory of wind generated waves. *J. Fluid Mech.* **14**, 385–397.

LIGHTHILL, M. J. 1978 *Waves in Fluids.* Cambridge University Press.

LONGUET-HIGGINS, M. S. 1969 Action of a variable stress at the surface of water waves. *Phys. Fluids* **12**, 737–740.

LONGUET-HIGGINS, M. S. & COKELET, E. D. 1976 The deformation of steep surface waves. I. A numerical method of computation. *Proc. R. Soc. Lond.* A **350**, 1–26.

LONGUET-HIGGINS, M. S. & STEWART, R. W. 1960 Changes in the form of short gravity waves on long waves and tidal currents. *J. Fluid Mech.* **8**, 565–583.

MASON, P. J. & KING, J. C. 1985 Measurements and predictions of flow and turbulence over an isolated hill of low slope. *Q. J. R. Met. Soc.* **111**, 617–640.

MILES, J. W. 1957 On the generation of surface waves by shear flows. *J. Fluid Mech.* **3**, 185–204.

MILES, J. W. 1967 On the generation of surface waves by shear flows. Part 5. *J. Fluid Mech.* **30**, 163–175.

PHILLIPS, O. M. 1957 On the generation of waves by a turbulent wind. *J. Fluid Mech.* **2**, 417–445.

PHILLIPS, O. M. 1977 *Dynamics of the Upper Ocean.* Cambridge University Press.

PHILLIPS, O. M. & BANNER, M. L. 1974 Wave breaking in the presence of wind drift and swell. *J. Fluid Mech.* **66**, 625–640.

PLANT, W. J. 1984 A relationship between wind shear stress and wave slope. *J. Geophys. Res.* **87**, C3, 1961–1967.

RAMAMONJIARISOA, A. 1974 Contribution a l'étude de la structure statistique et des mechanismes de génération des vagues de vent. Thesis, Universitié de Provence (also *IMST* no. AO 10023).

SMITH, F. T., BRIGHTON, P. M. W., JACKSON, P. S. & HUNT, J. C. R. 1981 On boundary layer flow past two dimensional bodies. *J. Fluid Mech.* **113**, 123–152.

SNYDER, R. L., DOBSON, F. W., ELLIOT, J. A. & LONG, R. B. 1981 Array measurements of atmospheric pressure fluctuations above gravity waves. *J. Fluid Mech.* **102**, 1–59.

STEWART, R. W. 1969 Mechanics of the air sea interface. *Phys. Fluids Suppl.* **10**, 547–554.

SYKES, R. I. 1980 An asymptotic theory of incompressible turbulent flow over a small hump. *J. Fluid Mech.* **101**, 647–670.

TOWNSEND, A. A. 1965 Self-preserving flow inside a turbulent boundary layer. *J. Fluid Mech.* **22**, 773–797.

TOWNSEND, A. A. 1972 Flow in a deep turbulent boundary layer over a surface distorted by water waves. *J. Fluid Mech.* **55**, 719–735.

TOWNSEND, A. A. 1980 Sheared turbulence and additional distortion. *J. Fluid Mech.* **98**, 171–191.

WALMSEY, J. L., TAYLOR, P. A. & KEITH, Y. 1986 A simple model of neutrally stratified boundary layer flow over complex terrain with surface roughness modulation. *Boundary-Layer Met.* **36**, 157–186.

WU, J. 1968 Laboratory studies of wind–wave interactions. *J. Fluid Mech.* **34**, 91–112.

WU, J. 1975 Wind-induced drift currents. *J. Fluid Mech.* **68**, 49–70.

WU, J. 1979 Distribution and steepness of ripples on carrier waves. *J. Phys. Oceanogr.* **9**, 1014–1021.

ZEMAN, O. & JENSSEN, N. O. 1987 Modification to turbulence characteristics in flow over hills. *Q. J. R. Met. Soc.* **113**, 55–80.